AIMS Mathematics, 7(10): 18416–18449.
DOI: 10.3934/math.20221014
Received: 07 July 2022
Revised: 31 July 2022
Accepted: 03 August 2022
Published: 17 August 2022

http://www.aimspress.com/journal/Math

Research article

Nonlinear Boussinesq and Rosseland approximations on 3D flow in an interruption of Ternary nanoparticles with various shapes of densities and conductivity properties

Kiran Sajjan[1,†], Nehad Ali Shah[2,†], N. Ameer Ahammad[3], C.S.K. Raju[1], M. Dinesh Kumar[1], Wajaree Weera[4,*]

[1] Department of Mathematics, GITAM School of Science, GITAM Deemed to be University, Bangalore-Campus, Karnataka-562163
[2] Department of Mechanical Engineering, Sejong University, Seoul 05006, South Korea
[3] Department of Mathematics, Faculty of Science, University of Tabuk, P.O. Box741, Tabuk 71491, Saudi Arabia
[4] Department of Mathematics, Faculty of Science, Khon Kaen University, Khon Kaen, 40002, Thailand

* **Correspondence:** Email: wajawe@kku.ac.th.

† These authors contributed equally to this work and are co-first authors.

Abstract: In current days, hybrid models have become more essential in a wide range of systems, including medical treatment, aerosol particle handling, laboratory instrument design, industry and naval academia, and more. The influence of linear, nonlinear, and quadratic Rosseland approximations on 3D flow behavior was explored in the presence of Fourier fluxes and Boussinesq quadratic thermal oscillations. Ternary hybrid nanoparticles of different shapes and densities were also included. Using the necessary transformation, the resulting partial differential system is transformed into a governing ordinary differential system, and the solution is then furnished with two mixed compositions (Case-I and Case-II). Combination one looked at aluminum oxide (Platelet), graphene (Cylindrical), and carbon nanotubes (Spherical), whereas mixture two looked at copper (Cylindrical), copper oxide (Spherical), and silver oxide (Platelet). Many changes in two mixture compositions, as well as linear, quadratic, and nonlinear thermal radiation situations of the flow, are discovered. Case-1 ternary combinations have a wider temperature distribution than Case-2 ternary mixtures. Carbon nanotubes

(Spherical), graphene (Cylindrical), and aluminum oxide (Platelet) exhibit stronger conductivity than copper oxide (Spherical), copper (Cylindrical), and silver oxide (Platelet) in Case 1. (Platelet). In copper oxide (Spherical), copper (Cylindrical), and silver (Platelet) compositions, the friction factor coefficient is much higher. The combination of liquids is of great importance in various systems such as medical treatment, manufacturing, experimental instrument design, aerosol particle handling and naval academies, etc. Roseland's quadratic and linear approximation of three-dimensional flow characteristics with the existence of Boussinesq quadratic buoyancy and thermal variation. In addition, we combine tertiary solid nanoparticles with different shapes and densities. In many practical applications such as the plastics manufacturing and polymer industry, the temperature difference is remarkably large, causing the density of the working fluid to vary non-linearly with temperature. Therefore, the nonlinear Boussinesq (NBA) approximation cannot be ignored, since it greatly affects the flow and heat transport characteristics of the working fluid. Here, the flow of non-Newtonian elastomers is controlled by the tension of an elastic sheet subjected to NBA and the quadratic form of the Rosseland thermal radiation is studied.

Keywords: three-dimensional flow; Boussinesq approximation (nonlinear); quadratic thermal radiation of Rosseland; Graphene, CNT, copper, Aluminum, silver particles, ternary hybrid nanofluid; spherical, cylindrical and platelet, etc.
Mathematics Subject Classification: 76-10, 76R10

1. Introduction

A Nanofluid is a liquid that contains nanoparticles, which are particles that are more modest than a nanometer. These liquids are nanoparticle colloidal suspensions in a base liquid that have been made. Metals, oxides, carbides, and carbon nanotubes are the most well-known nanoparticles used in nanofluids. Water and ethylene glycol are normal essential liquids. Nanofluids' rheological conduct is found to be vital in deciding their propriety for convective warmth move applications. Nanofluids are mostly used as coolants in heat move gear, for example, heat exchangers and electronic cooling frameworks due to their presence in warm attributes. With more command over the conduct of the delivered liquid, half nanofluids offer extensive potential in thermodynamic applications. Ahmed Sameh et al. [1] found that expanding the curve boundary builds the intricacy of the stream area, bringing down both the nanofluid movement and the warmth move rate. They likewise found that high Reynolds numbers and Rayleigh numbers lead to high average Nusselt esteems. Ayub Assad, et al. [2] tracked down that expanding the effect of homogeneous response gives higher fixation and that expanding the tendency point gives lower energy transmission of 3-D Hybrid Nanofluid because of Lorentz power. Basha et al. [3] tracked down that expanding the blended convection boundary brings down the digression exaggerated nanofluid temperature and brings down the nanofluid velocity. They additionally checked out how the pace of warmth and mass transmission is quicker at ξ =0 than it is at ξ=1. At the point when authentic hazy diesel fuel beads are approximated as dark obscure circles, the impact of warm radiation on warming and dissipation is substantially less, as per Dombrovsky et al. [4]. Elshehabey et al. [5] tracked down that expanding the Hartmann number brings down liquid movement, isotherms appropriations, and greatest upsides of nearby entropy creation inferable from heat move, and neighborhood entropy age because of liquid grinding, and the normal Nusselt number. They

likewise found that expanding the opening length works on regular convection, which assists with supporting the warmth move rate. As indicated by Kumar et al. [6], studied the linear and quadratic convection on 3D flow with transpiration and hybrid nanoparticles. Kabashnikov and Kmit [7] discovered a condition for the normal warm radiation force of a level layer that incorporates violent temperature throbs and is named a Gaussian interaction. Mahanthesh and Mackolil [8] tracked down that the adjusted Buongiorno model works on the liquid velocity and temperature field, that the quadratic warm radiative factor is more successful than the straight radiative factor, and that Brownian irregular movement and thermophoresis increase the temperature profile. Mahanthesh et al. [9] investigated this. By raising the radiation part of the warm field, and by expanding the mass convergence of residue particles, both liquid velocity and temperature profiles break down. The numerical simulation of a thermally enhanced EMHD flow of a heterogeneous micropolar mixture comprising (60%)-ethylene glycol (EG), (40%)-water (W), and copper oxide nanomaterials (CuO) by Shah et al. [10]. Warmth engendering and liquid stream rate in the gadget are both helped by temperature contrasts. At the point attractions are negligible, Elnaqeeb et al. [11] tracked down that the temperature circulation is greatest while heat transmission is minima in ternary-crossover nanofluids comprised of the small thickness of nanoparticles. When contrasted with Rosseland quadratic warm radiation and Rosseland straight warm radiation, Al-Kouz, Wael, et al. [12] tracked down that the temperature of viscoelastic material is higher attributable to the course of Rosseland nonlinear warm radiation. The adjustment is a traditional guess for lightness-driven progressions of thick, incompressible liquids with temperatures at the plate and distant from the plate, as per Mahanthesh [13]. It was found that the quadratic convection term inconsequentially affects the velocity profile with time variety.

The impacts of dissolving heat move and non-direct warm radiation in polarized nanofluid vehicles utilizing CNTs across a quadratic extended sheet are explored. Blended convection (consolidated free and constrained convection) transitions are utilized in an assortment of utilizations, including cooling electronic frameworks, sun-oriented warm frameworks, drying cycles, and warmth exchangers. The warm field is brought down with expanding dissolving and warm unwinding numbers, as indicated by Muhammad Taseer et al. [14]. The warm profile was brought down to consider more exact volume part computations of nanoparticles, while the warmth source-sink boundary and the warmth source-sink boundary were expanded. The Brinkman number, as indicated by Naveen and Ram Reddy [15], builds the thickness of the warm and force limit layers inside the channel while diminishing the thickness of the focus limit layer. In the examples when the warmth limit of base liquids is bigger than that of nanoparticles, Okonkwo et al. [16] tracked down that expanding nanoparticle volume fixation causes a decrease in the particular warmth limit of nanofluids. Coolants should have a bigger warmth limit. Palani and Abbas [17] tracked down that a Mathematical model for temperamental convection heat transport from an upward plate with consolidated impacts of MHD and warm radiation might be utilized. They found that as the warmth radiation boundary (or) the attractive field boundary M declines, the velocity rises. Due to an expansion in warm radiation, the dimensionless temperature is relied upon to drop. As indicated by Srinivasacharya et al. [18], the effects of nonlinear temperature and fixation factors on warmth and mass vehicle are more articulated in the Darcy permeable medium than in the non-Darcy permeable medium.

The Boussinesq estimate expresses that while the distinction in inactivity is little, gravity is adequately amazing to make the particular loads of the two liquids vary altogether. The Boussinesq estimate is utilized to tackle issues including liquid stream and warmth move where the temperature

of the liquid changes starting with one area then onto the next. Mass, force, and energy are completely saved in the liquid. Varieties in liquid qualities other than thickness are ignored in the Boussinesq estimation, and thickness arises just when it is increased by gravity's velocity increase. The quadratic convective progression of half and half nanofluid in an annulus presented to quadratic warmth radiation was investigated interestingly by Thriveni and Mahanthesh [19]. They took a gander at the impacts of attractions/infusion and uniform ring development and tracked down that quadratic warm radiation greater affected velocity and temperature dispersions than straight warm radiation. Moreover, an ascent in quadratic convection and quadratic warmth radiation further develops the skin's grating coefficient on the external annulus' inward surface. As per Thriveni and Mahanthesh [20], the temperature profile of crossover nanofluid is more noteworthy than that of mono nanofluid, trailed by base liquid, and the expansion of composite nanoparticles extensively further develops the temperature profile. Because of the presence of the pull boundary, which might affect the warmth move effectiveness, Zainal et al. [21] tracked down that the customary Al2O3-H2O nanofluid has a more prominent pace of warmth move than the half and half Al2O3-Cu/H2O nanofluid. In the field of lightness driven stream in liquid elements, the Boussinesq estimate is used. It disregards thickness varieties besides in wording increased by gravity's velocity increase. Dostalk et al. [22] examined the subjective properties of warm convection in a two-dimensional climate for marginally supercritical Rayleigh numbers. Jha, Basant, and Michael [23] examined the impact of the nonlinear Boussinesq estimate on blended convection stream in an upward channel with deviated divider warming and created and coordinated the administering condition consolidating the nonlinearity into the energy condition. Within the sight of non-direct Boussinesq estimation and warm definition with convective limit conditions, Kameswaran et al. [24] revealed that two-dimensional limit layer nanofluid stream across a vertical undulating surface immersed a non-Darcy permeable medium. As per Krishnani et al. [25], the temperature shape anticipated by the Boussinesq model for some random cross-segment is symmetric, decreasing the impact of neighborhood convection. John et al. [26] found that expanding variable warm conductivity and diffusivity builds the utilization of more liquid particles, in this manner expanding the force field and that both straight and nonlinear Boussinesq approximations advanced the velocity field while diminishing the focus and energy fields. The subjective conduct of straight and quadratic Boussinesq approximations for the variety of actual boundaries is comparative, as per Sunday Iyiola Opadiran and Samuel Segun Okoya [27], and their examination uncovered that the impact of warm conductivity increments for both straight and quadratic models, with expanding the consistency (warm conductivity) boundary prompting an increment in the normal Nusselt number. The nonlinear Boussinesq estimate is considered in the investigation of warmth and mass exchange cycles of an Ostwald-de Waele model force law liquid stream across a convectively warmed slanted plate in a non-Darcy permeable medium by Ram Reddy et al. [28]. The altered Buongiorno model was utilized to explore the volume level of NPs, arbitrary development of NPs, and the thermophoresis interaction, as indicated by Rana Puneet et al. [29]. The quadratic Boussinesq estimate works with the improvement of the force limit layer and rushes the warmth transport rate at the plate. The nanofluid temperature field and its limit layer are sped up by a quadratic warm radiative warmth stream. In contrast with the Boussinesq case, Vasu et al. [30] tracked down that expanding the nonlinear temperature boundary (i.e., non-Boussinesq case) increments both warmth move and mass exchange rates while expanding the thermophoresis boundary diminishes heat move rate (Nusselt number) and mass exchange rate. They acquired this when the temperature was diminished, yet the centralization of nanoparticles rose significantly as the Schmidt number climbed. Numerical and sensitivity

computations of three-dimensional flow and The radiant heat flux in RNTR is determined using the Rosseland approximation with this nonlinear Boussinesq approximation was studied by Rana et al. [36–39], Marangoni convection in a nanoliquid flowing on an infinite disk is studied numerically by Puneet Rana and Gaurav Gupta.

To obtain analytical solutions for the flow variables, the least square technique (LSM) is applied. In an experimental situation where the values of both variables are susceptible to basically unknown errors, the challenge of using statistical methods to identify the optimal linear connection of the type Y = AX +B was investigated. The size of the slope A is underestimated by traditional least-squares regression analysis in this circumstance. A simple approach for calculating the appropriate slope and intercept value has been given when both variables include errors which is explained by [40–43].

In view of the aforementioned infestations, there is no study reported on Nonlinear Boussinesq and Rosseland approximations on 3Dimensional flow in an interruption of Ternary nanoparticles with various shapes of densities and conductivity properties. The Fourier flux is taken into account. The arising partial governing system is transformed into ordinary differential systems and then solved numerically via plotting graphs and tables. We also validated the present study with existing studies by considering the limited situation.

2. Mathematical formulation

Inside a rectangular closed zone, the transport mechanisms of water-moving nanoparticles with a reduced density and a significant broad nanoparticle density of diverse shapes are studied. The order of argument proposed by Prandtl [31] and the concept of stretching at the wall proposed by Sakiadis [32] were used to model the boundary layer flow of water transporting three different nanoparticles (types and shapes to form a single ternary hybrid nanofluid each) through a rectangular closed domain. As a consequence, the simplified Navier-Stoke equation was used, together with appropriate models for the thermophysical properties of the working fluid (Figure 1).

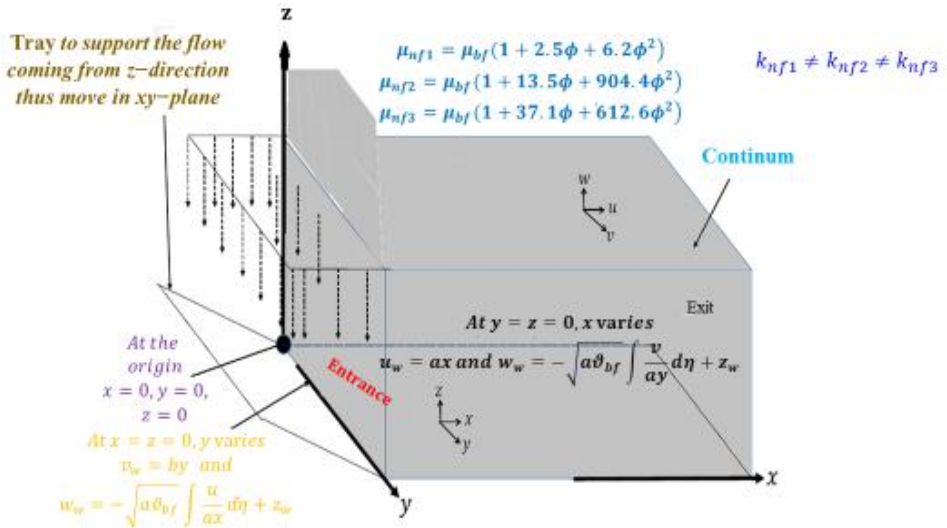

Figure 1. Physical Configuration in *XYZ*-domain.

The governing equation for modeling laminar and incompressible three-dimensional flows in the region where the flow is steady and viscosity has a major impact is presented in this section. $u_w(x) = ax$ and $v_w(x) = by$ are the x-and y-direction stretching velocity of the fluid layer next to horizontal surfaces, respectively. The dimensional governing equation for modeling the transport phenomena, according to Nehad et al. [33], is of the form
Equation of Continuity:

$$\left(\frac{\partial w}{\partial z}\right)+\left(\frac{\partial v}{\partial y}\right)+\left(\frac{\partial u}{\partial x}\right)=0 \tag{1}$$

Momentum equation:

$$\rho_{hnf}\left[w\left(\frac{\partial u}{\partial z}\right)+v\left(\frac{\partial u}{\partial y}\right)+u\left(\frac{\partial u}{\partial x}\right)\right]=\mu_{hnf}\frac{\partial^2 u}{\partial z^2}+g[(\rho\beta_o)_{hnf}(T-T_\infty)+(T-T_\infty)^2(\rho\beta_1)_{hnf}], \tag{2}$$

$$\rho_{hnf}\left[w\left(\frac{\partial v}{\partial z}\right)+v\left(\frac{\partial v}{\partial y}\right)+u\left(\frac{\partial v}{\partial x}\right)\right]=\mu_{hnf}\frac{\partial^2 v}{\partial z^2}+g[(\rho\beta_o)_{hnf}(T-T_\infty)+(\rho\beta_1)_{hnf}(T-T_\infty)^2], \tag{3}$$

Energy equation with RLTR:

$$\left[w\left(\frac{\partial T}{\partial z}\right)+v\left(\frac{\partial T}{\partial y}\right)+u\left(\frac{\partial T}{\partial x}\right)\right]=\frac{k_{hnf}}{(\rho c_p)_{hnf}}\frac{\partial^2 T}{\partial z^2}+\frac{\partial^2 T}{\partial z^2}\left(\frac{16\sigma^*}{3k^*}\left(\frac{T_\infty^3}{\rho c_p}\right)\right), \tag{4}$$

Energy equation with RNTR:

$$\left[w\left(\frac{\partial T}{\partial z}\right)+v\left(\frac{\partial T}{\partial y}\right)+u\left(\frac{\partial T}{\partial x}\right)\right]=\frac{k_{hnf}}{(\rho c_p)_{hnf}}\frac{\partial^2 T}{\partial z^2}+\frac{\partial}{\partial z}\left[\frac{16\sigma^*}{3k^*}T^3\frac{\partial T}{\partial z}\right], \tag{5}$$

The following boundary conditions are studied for the situation of three-dimensional flow due to stretching along the x- and y-axes where suction is substantial.
At $y = 0, z = 0$ along the x-axis are

$$w=w_w=(-\sqrt{a\vartheta_{bf}}\int\frac{v}{ay}d\eta+z_w),\ u=u_w(x)=ax, \tag{6}$$

$$\begin{aligned} &at\ z=0, and\ y=0\\ &as\ z\to\infty u\to 0, \end{aligned} \tag{7}$$

At $x = 0, z = 0$ along the y-axis are

$$w=w_w=(-\sqrt{a\vartheta_{bf}}\int\frac{v}{ay}d\eta+z_w), v=v_w(x)=by, \tag{8}$$

$$\begin{aligned} &at\ z=0, and\ x=0\\ &v\to 0, as\ \ z\to\infty\ and\ x=0 \end{aligned} \tag{9}$$

Eq. (4)'s boundary conditions are as follows:

$$at\ z=0\ T=T_w \quad as(x,y)\to\infty \tag{10}$$

$$as\ z\to\infty,\ T\to T_\infty,\ \ and\ (x,y)\to\infty \tag{11}$$

The physical quantities of fluid dynamics, the Nusselt number, and local skin friction coefficients are defined as

$$\left.\begin{aligned} Nu_x &= \frac{-xk_{hnf}}{(T_w-T_\infty)k_{bf}}\left(\frac{\partial T}{\partial z}\right)\Big|_{z=0}, c_{fx}=\frac{\mu_{hnf}}{\rho_{bf}a^2x^2}\left(\frac{\partial u}{\partial z}\right)\Big|_{z=0}\\ Nu_y &= \frac{-yk_{hnf}}{k_{bf}(T_w-T_\infty)}\left(\frac{\partial T}{\partial z}\right)\Big|_{z=0}, c_{gy}=\frac{\mu_{hnf}}{\rho_{bf}a^2y^2}\left(\frac{\partial v}{\partial z}\right)\Big|_{z=0} \end{aligned}\right\} \tag{12}$$

The viscosity and thermal conductivity of ternary hybrid nanoparticles are measured.

$$\left.\mu_{hnf}=\frac{\phi_3\mu_{nf3}+\phi_2\mu_{nf2}+\phi_1\mu_{nf1}}{\phi},\ k_{hnf}=\frac{k_{nf3}\phi_3+k_{nf2}\phi_2+k_{nf1}\phi_1}{\phi}\right\} \tag{13}$$

The form of nanoparticles was determined using several models for viscosity and thermal conductivity of spherical, cylindrical, and platelet nanoparticles. Because the form of nanoparticles influences their density, this was required for a viable model. Higher-density nanoparticles have a nanofluid with variable viscosity and thermal conductivity.

The densities model for ternary hybrid nanoparticles is

$$\rho_{hnf}=(1-\phi_3-\phi_2-\phi_1)\rho_{bf}+\phi_1\rho_{sp1}+\phi_2\rho_{sp2}+\phi_3\rho_{sp3} \tag{14}$$

The equation can be used to calculate the heat capacities of a ternary hybrid nanofluid.

$$(\rho c_p)_{hnf}=(1-\phi_3-\phi_2-\phi_1)(\rho c_p)_{bf}+\phi_1(\rho c_p)_{sp1}+\phi_2(\rho c_p)_{sp2}+\phi_3(\rho c_p)_{sp3} \tag{15}$$

The viscosity and thermal conductivity models for spherical, cylindrical, and platelet nanoparticles are as follows

$$\left.\begin{aligned} &\frac{\mu_{nf1}}{\mu_{bf}}=1+2.5\phi+6.2\phi^2\\ &k_{nf1}=k_{bf}\left[\frac{k_{sp1}+2k_{bf}-2\phi(k_{bf}-k_{sp1})}{k_{sp1}+2k_{bf}+\phi(k_{bf}-k_{sp1})}\right] \end{aligned}\right\} \tag{16}$$

$$\left.\begin{aligned}&\frac{\mu_{nf2}}{\mu_{bf}}=1+13.5\phi+904.4\phi^2\\&k_{nf2}=k_{bf}\left[\frac{k_{sp2}+3.9k_{bf}-3.9\phi(k_{bf}-k_{sp2})}{k_{sp2}+3.9k_{bf}+\phi(k_{bf}-k_{sp2})}\right]\end{aligned}\right\} \tag{17}$$

$$\left.\begin{aligned}&\frac{\mu_{nf3}}{\mu_{bf}}=1+37.1\phi+612.6\phi^2\\&k_{nf3}=k_{bf}\left[\frac{k_{sp3}+4.7k_{bf}-4.7\phi(k_{bf}-k_{sp3})}{k_{sp3}+4.7k_{bf}+\phi(k_{bf}-k_{sp3})}\right]\end{aligned}\right\} \tag{18}$$

Given that spherical nanoparticles have a volume of 1, cylindrical nanoparticles have a volume of 2, and platelet nanoparticles have a volume of 3, then, the percentage of total volume is

$$\phi=\phi_1+\phi_2+\phi_3 \tag{19}$$

Models with different thermal properties Eqs (16)–(18) indicate that it is suitable for ternary hybrid nanofluids with $\phi > 0.02$ value. Using the stretching ratio c, the suction parameter f_w, and the variables, a solution of the model expressed as Eq (1)–(12) was found.

$$\left.\begin{aligned}&\eta=z\left(\frac{a}{\vartheta_{bf}}\right)^{\frac{1}{2}},\ c=\frac{b}{a},\ f_w=\frac{-z_w}{\sqrt{a\vartheta_{bf}}},\ \theta=\frac{T-T_\infty}{T_w-T_\infty},u=ax\frac{df}{d\eta},v=by\frac{dg}{d\eta},\\&w=-\left(a\vartheta_{bf}\right)^{\frac{1}{2}}\left[f(\eta)+cg(\eta)\right],(T_w-T_\infty)=bx\end{aligned}\right\} \tag{20}$$

$$\left.\begin{aligned}&A_2=1-\phi_1-\phi_2-\phi_3+\phi_1\frac{\rho_{sp1}}{\rho_{bf}}+\phi_2\frac{\rho_{sp2}}{\rho_{bf}}+\phi_3\frac{\rho_{sp3}}{\rho_{bf}},B_1=1+2.5\phi+6.2\phi^2,\\&B_2=1+13.5\phi+904.4\phi^2,\\&B_3=1+37.1\phi+612.6\phi^2,\ B_4=\frac{k_{sp1}+2k_{bf}-2\phi(k_{bf}-k_{sp1})}{k_{sp1}+2k_{bf}+\phi(k_{bf}-k_{sp1})},\\&B_5=\frac{k_{sp2}+3.9k_{bf}-3.9\phi(k_{bf}-k_{sp2})}{k_{sp2}+3.9k_{bf}+\phi(k_{bf}-k_{sp2})},B_6=\frac{k_{sp3}+4.7k_{bf}-4.7\phi(k_{bf}-k_{sp3})}{k_{sp3}+4.7k_{bf}+\phi(k_{bf}-k_{sp3})},\\&A_1=B_1\phi_1+B_2\phi_2+B_3\phi_3,\quad A_3=B_4\phi_1+B_5\phi_2+B_6\phi_3,\\&A_4=1-\phi_1-\phi_2-\phi_3+\phi_1\frac{(\rho c_p)_{sp1}}{(\rho c_p)_{bf}}+\phi_2\frac{(\rho c_p)_{sp2}}{(\rho c_p)_{bf}}+\phi_3\frac{(\rho c_p)_{sp3}}{(\rho c_p)_{bf}},\\&E=1-\phi_1-\phi_2-\phi_3+\phi_1\frac{\rho_{sp1}/\beta_{sp1}}{\rho_{bf}/\beta_{bf}}+\phi_2\frac{\rho_{sp2}/\beta_{sp2}}{\rho_{bf}/\beta_{bf}}+\phi_3\frac{\rho_{sp3}/\beta_{sp3}}{\rho_{bf}/\beta_{bf}},\end{aligned}\right\} \tag{21}$$

The collection of dimensionless governing equations now has the following shape: (see Elnaqeeb et al. [11], Al-Kouz et al. [12], M. Dinesh Kumar et al. [32],);

$$\frac{A_1}{A_2\phi}\frac{d^3f}{d\eta^3}-\frac{df}{d\eta}\frac{df}{d\eta}+\left[f+cg\right]\frac{d^2f}{d\eta^2}+\lambda E\left[\theta Q_c\left(1+\theta\right)\right]=0 \tag{22}$$

$$\frac{A_1}{A_2\phi}\frac{d^3g}{d\eta^3}-c\frac{dg}{d\eta}\frac{dg}{d\eta}+\left[f+cg\right]\frac{d^2g}{d\eta^2}+\lambda E\left[\theta Q_c\left(1+\theta\right)\right]=0 \tag{23}$$

The Rosseland thermal radiation mechanism in the thermal analysis was investigated by two methods.

1) Rosseland nonlinear thermal radiation (RNTR)

2) Rosseland Linear thermal radiation (RLTR)

RLTR Energy Equation

$$\left[\frac{A_3}{A_4\phi}+\frac{4R}{3}\right]\frac{d^2\theta}{d\eta^2}+\Pr\left[f+cg\right]\frac{d\theta}{d\eta}=0 \tag{24}$$

RNTR Energy Equation

$$\left[\frac{A_3}{A_4\phi}+\frac{4R}{3}\left(\theta\left(\theta_p-1\right)+1\right)^3\right]\frac{d^2\theta}{d\eta^2}+\Pr\left[f+cg\right]\frac{d\theta}{d\eta}+4R\left(\theta_p-1\right)\left[\theta\left(\theta_p-1\right)+1\right]^2\frac{d\theta}{d\eta}\frac{d\theta}{d\eta}=0 \tag{25}$$

and the boundary condition are

$$\begin{aligned}&\eta=0,\ \frac{df\left(0\right)}{d\eta}=1,\ f\left(0\right)=f_w,\ \frac{dg\left(0\right)}{d\eta}=c,\ g\left(0\right)=\frac{f_w}{c},\\&as\ \eta\to 0,\ \frac{df}{d\eta}\to 0,\frac{dg}{d\eta}\to 0,\ \theta\to 0,\end{aligned} \tag{26}$$

Where $R=\frac{4\sigma^*T_\infty^3}{kk^*}$ is the quadratic thermal radiation parameter, $Q_c=\frac{\beta_1}{\beta_0}\left(T_w-T_\infty\right)$ is quadratic/nonlinear convection parameter $\lambda=\frac{Gr_x}{\mathrm{Re}_x^2}=\frac{gb\beta_0}{a^2}$ is the mixed convection parameter, $\theta_p=\frac{T_w}{T_\infty}$ is the temperature ratio parameter,

$$\begin{aligned}&f=f_1,\quad g=f_4,\quad \theta=f_7,\\&f'=f_2,\quad g'=f_5,\quad \theta'=f_8,\\&f''=f_3,\quad g''=f_6,\quad \theta''=f_8',\\&f'''=f_3',\quad g'''=f_6',\end{aligned}$$

The technique of superposition was adopted to reduced the boundary value problems Eqs (22)–(25) to an initial value problem Eq (26) of the form

$$f_1' = f_2,$$
$$f_2' = f_3,$$
$$f_3' = \frac{A_2\phi}{A_1}\left(\left(f_2\right)^2 - f_3[f_1 + cf_4] - \lambda E\left[f_7 Qc\left(1+ f_7\right)\right]\right),$$
$$f_4' = f_5,$$
$$f_5' = f_6,$$
$$f_6' = \frac{A_2\phi}{A_1}\left(c\left(f_5\right)^2 - f_6[f_1 + cf_4] - \lambda E\left[f_7 Qc\left(1+ f_7\right)\right]\right)$$
$$f_7' = f_8,$$
$$f_8' = \frac{-1}{\left[\frac{A_3}{A_4\phi} + \frac{4R}{3}\left(f_7\left(\theta_p - 1\right)+1\right)^3\right]}\left(\Pr\left[f_1 + cf_4\right] f_8 + 4R\left(\theta_p - 1\right)\left[f_7\left(\theta_p - 1\right)+1\right]^2 (f_8)^2\right)$$

$$\text{fa(1)=}f_w,\ \text{fa(2)=1},\ \ \text{fa(4)=}\frac{f_w}{c},\ \text{fa(5)=c, fa(7)=1,}$$
$$\text{fb(2)=0, fb(5)=0, fb(7)-0,}$$

The least square method is used to provide analytical solutions for the flow variables (LSM).

Skin Friction for Radiation parameter

$$Cf_{x_{case1}} = -0.03217R + 2.789746, \qquad Cf_{x_{case2}} = 0.113964R - 0.6553,$$
$$Cf_{y_{case1}} = 0.00814875R + 0.09790808, \quad Cf_{y_{case2}} = 0.0911046R + 0.73215$$

Skin Friction for Stretching rate ratio parameter

$$Cf_{x_{case1}} = -0.57123c - 2.48769, \qquad Cf_{x_{case2}} = -1.24866c - 0.28338,$$
$$Cf_{y_{case1}} = -0.79326c + 0.21802567, \quad Cf_{y_{case2}} = 1.651523c + 0.336694,$$

Skin Friction for temperature ratio parameter

$$Cf_{x_{case1}} = 0.484119\theta_p - 2.54493, \qquad Cf_{x_{case2}} = 1.368644\theta_p - 0.0898,$$
$$Cf_{y_{case1}} = 0.1439739\theta_p + 0.0977365, \quad Cf_{y_{case2}} = 0.404137\theta_p + 0.788014,$$

Nusselt number for suction velocity, mixed convection and Radiation parameter

Case -1

$$Nus_{linear} = 13.49106 f_w + 4.008559, \quad Nus_{Nonlinear} = 10.89012 f_w + 3.23575, \quad Nus_{Quadratic} = 16.37517 f_w + 4.865504,$$
$$Nus_{linear} = 2.919014R + 5.032223, \quad Nus_{Nonlinear} = 0.115213R + 5.305672, \quad Nus_{Quadratic} = 6.028067R + 4.729004,$$
$$Nus_{linear} = 0.084386\lambda + 6.601754, \quad Nus_{Nonlinear} = 0.068117\lambda + 5.329004, \quad Nus_{Quadratic} = 0.102426\lambda + 8.013069,$$

Case -2

$$Nus_{linear} = 13.50009 f_w + 4.165656, \quad Nus_{Nonlinear} = 10.91127 f_w + 3.366835, \quad Nus_{Quadratic} = 16.37076 f_w + 5.051446,$$
$$Nus_{linear} = 3.01085R + 5.124976, \quad Nus_{Nonlinear} = 0.128372R + 5.434511, \quad Nus_{Quadratic} = 6.207147R + 4.781742,$$
$$Nus_{linear} = 0.294077\lambda + 6.6423, \quad Nus_{Nonlinear} = 0.237684\lambda + 5.36855, \quad Nus_{Quadratic} = 0.35661\lambda + 8.054724,$$

3. Interoperation of physical quantities and their discussions

The got results to exhibit the impacts of non-dimensional administering boundaries like radiation boundary (R), dimensionless attractions velocity (f_w), extending rate proportion (c), nonlinear convection boundary (Q_c), blended convection boundary (λ), volume part of the ternary crossover nanofluid (ϕ), temperature proportion boundary (θ_p) on dimensionless profiles $f(\eta), f'(\eta), g(\eta), g'(\eta)$ and $\theta(\eta)$, skin friction coefficients in *x* and y directions (Cf_x, Cf_y) as well as Nusselt number (*Nu*). (See Figures 2–21 and Tables 2–4). The default boundary esteems utilized in the reenactments are Pr =7.2, ϕ=0.05, R=0.5, Q_c=0, $\theta_p = 0.2$, c=0.2, λ=0.5, and f_w=0.2. Aside from the various qualities given in the pertinent figure and table, these qualities were kept consistent all through the examination. For three sorts of Rosseland warm radiation, the idea of velocities (pivotal velocity field $f'(\eta), g'(\eta)$, with *x* and *y* bearings separately) and temperature θ (η) is shown for Case-I and Case-II. In this investigation, we considered the Case-I composition is Graphene (Cylindrical), Carbon nanotubes (Spherical), and aluminum oxide (Platelet) as well as Case-II mixture is copper (Cylindrical), silver (Platelet), and copper oxide (Spherical).

The impact of a quadratic warm radiation boundary (R) on velocity in the *x*-direction and temperature is displayed in Figures 2 and 3 for both the Case-I and Case-II of the flow. An ascent in R reinforces the thickness of the warm obstruction, bringing about a temperature profile help. Besides, the warm radiation measure adds warmth to the viscoelastic liquid framework, causing the temperature profile to ascend as R increments. The impacts of dimensionless pull velocity (f_w) on velocities ($f'(\eta), g'(\eta)$) and temperature profiles are portrayed in Figures 4–6 for both the Case-I and Case-II of the flow. It has been found that expanding the dimensionless pull velocity of nanoparticles brings down the velocity and temperature profile of the two liquids. At the point when the pull at the divider is high, lesser temperature appropriation is conceivable close to the divider. Because of the expansion in attractions, the temperature dispersion lessens. It is noted that the distribution of velocity in the *x*-direction is higher in Case-I compared to Case-II. It happened due to the amalgamation of the particles (Graphene (Cylindrical), Carbon nanotubes (Spherical), and aluminum oxide (Platelet)) faster in Case-I. Figures 7–9 portray the impact of the proportion of extending rate boundary (c) on velocity and temperature profiles for both the Case-I and Case-II of the flow. The velocity profiles of liquid in the *y*-bearing ascent as the proportion of extending rate boundary increments however, the temperature profiles and velocity profiles of liquid in *x* way drop as the proportion of extending rate boundary increments.

The nonlinear convection boundary (Q_c) affects the velocity and temperature profiles, as found in Figures 10–12 for both the Case-I and Case-II of the flow. The impacts of Q_c on $f'(\eta), g'(\eta)$ and θ (η) are individually indistinguishable from those figures. This happened because of the quadratic warm convection term and it is a deduction from of the lightness power term. Figures 13–15 shows the effect of the mixed convection boundary (λ) on velocity and temperature profiles for both the Case-I and Case-II of the flow. Since the mixed convection boundary λ is contrarily identified with the thick power and straightforwardly identified with the vertical power of lightness, the velocity field is upgraded. Besides, the temperature profile is diminished because of a steady ascent in the warm differential with λ. The impact of the volume fraction of nanoparticles of the ternary cross breed nanofluid (ϕ) on velocity and temperature profiles is portrayed in Figsure 16–18 for both the Case-I and Case-II of the flow. The information shows that expanding the Volume division boundary of the ternary cross breed nanofluid lessens the liquid velocity profiles while expanding the temperature

profiles. The impact of the temperature proportion boundary (θ_p) on velocity and temperature profiles is found in Figures 19–21 for both the Case-I and Case-II of the flow. Clearly raising the temperature proportion boundary raises both velocity and temperature profiles. This may be attributable to the stream's expanded warm conductivity. It is interesting to mention that the Case-II composition has less distribution of temperature, whereas velocity is higher compared to the Case-I composition. It tells clearly about industrial needs one can select either Case-I mixture or Case-II mixtures respectively.

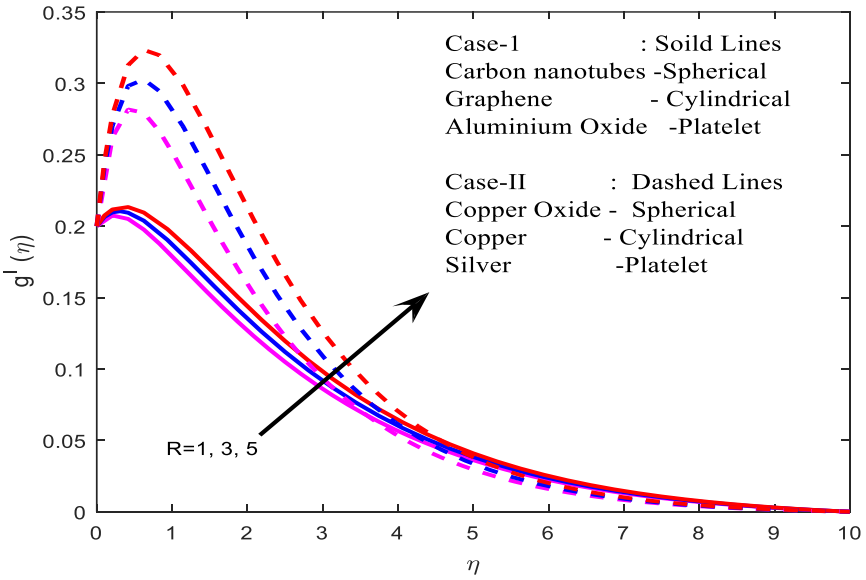

Figure 2. Velocity profiles for various R values.

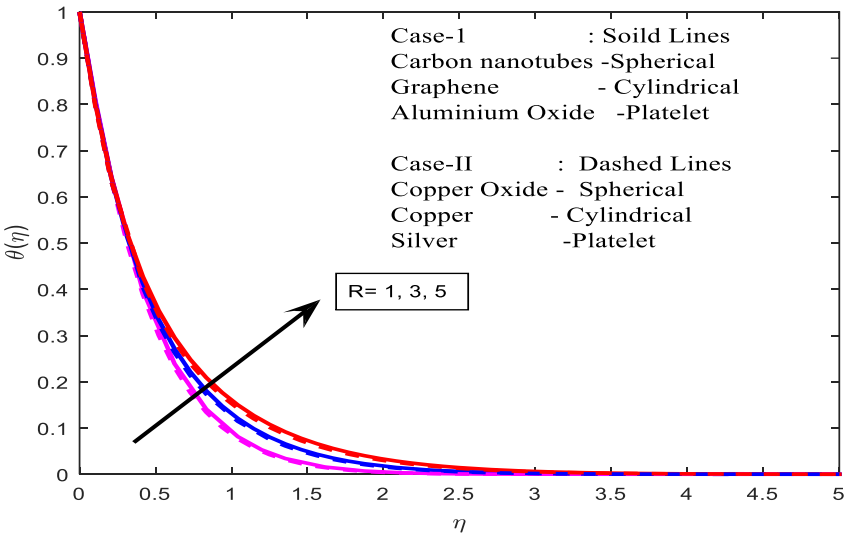

Figure 3. shows temperature curves for various R values.

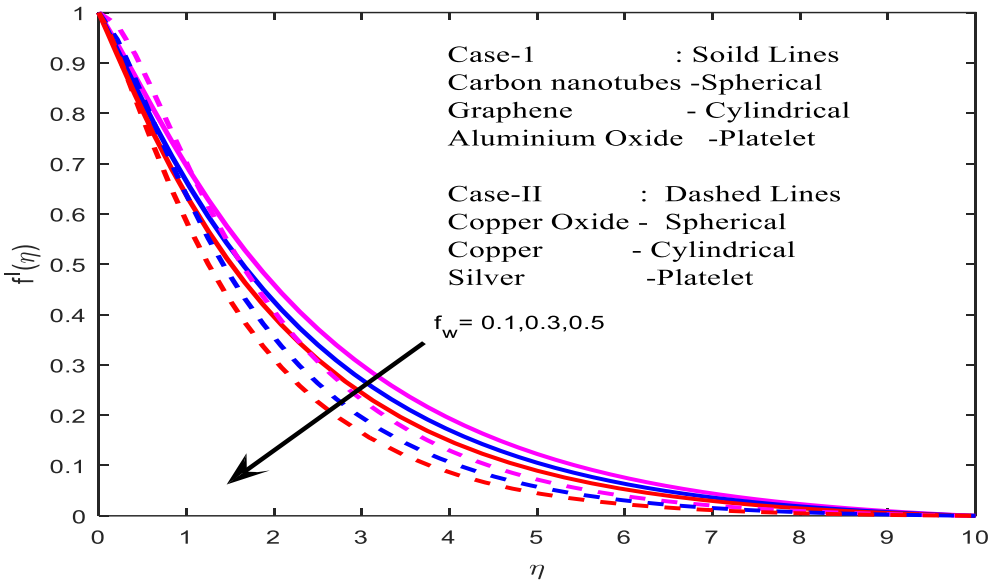

Figure 4. shows velocity profiles for various f_w values.

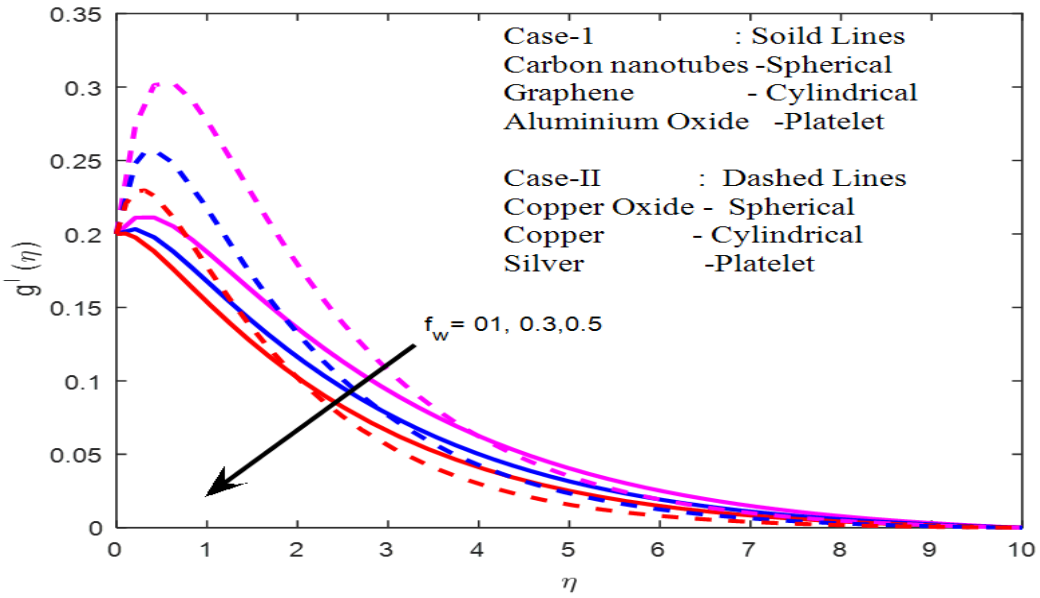

Figure 5. shows velocity profiles for various f_w values.

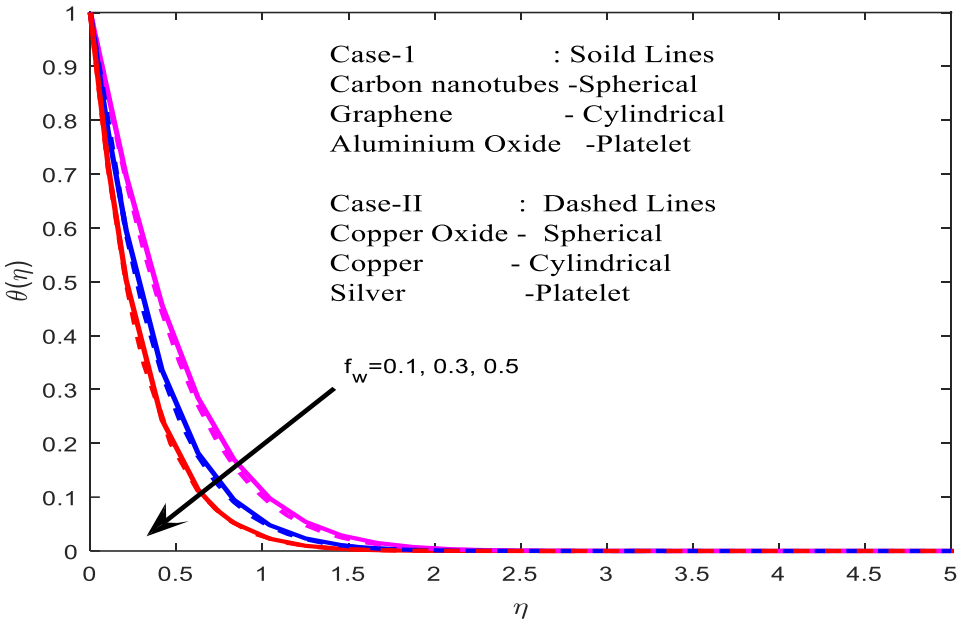

Figure 6. Temperature profiles at various f_w values.

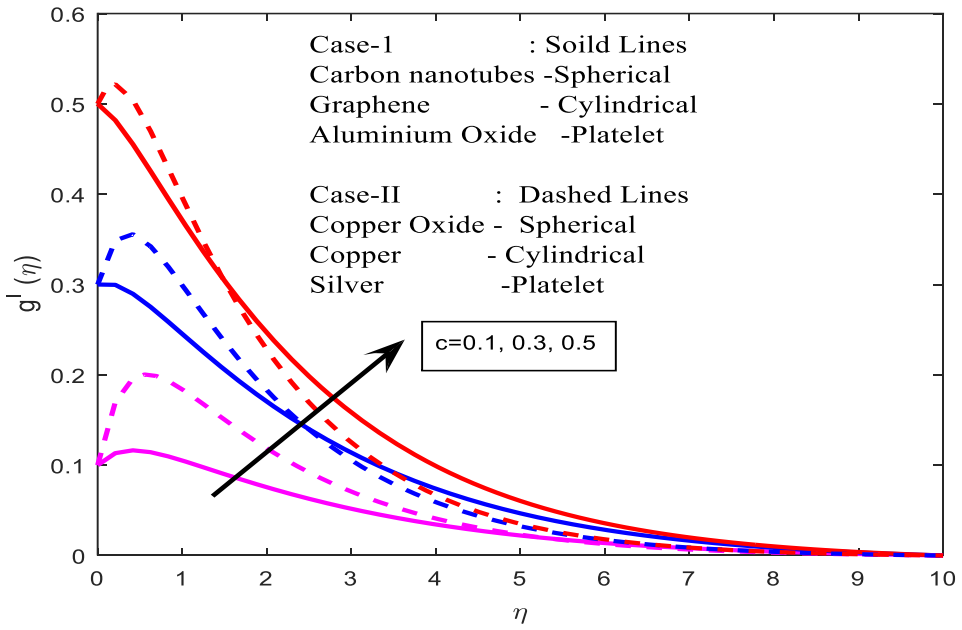

Figure 7. Velocity profiles for various c values.

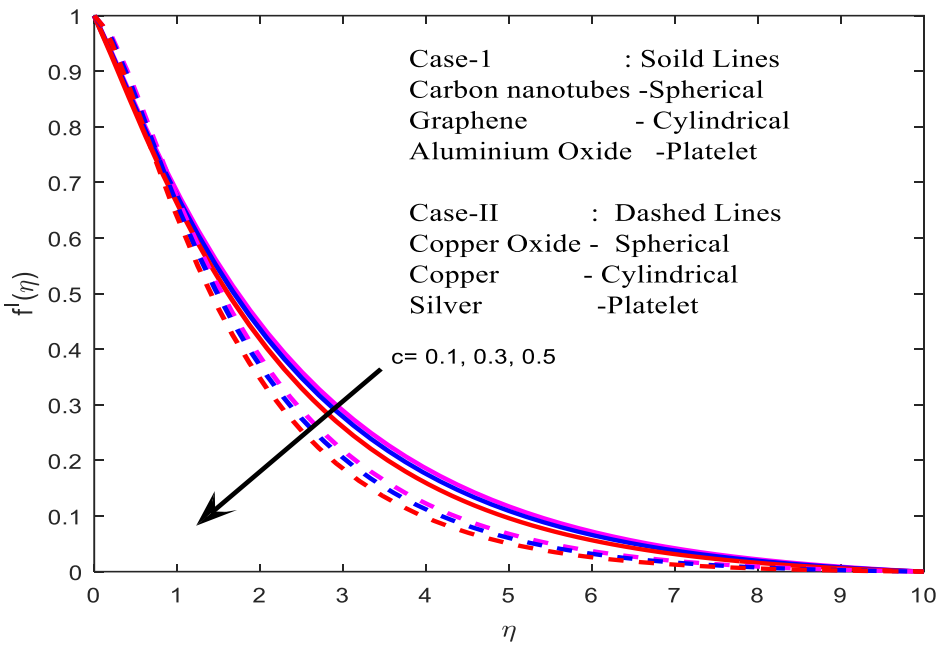

Figure 8. Velocity profiles for various c values.

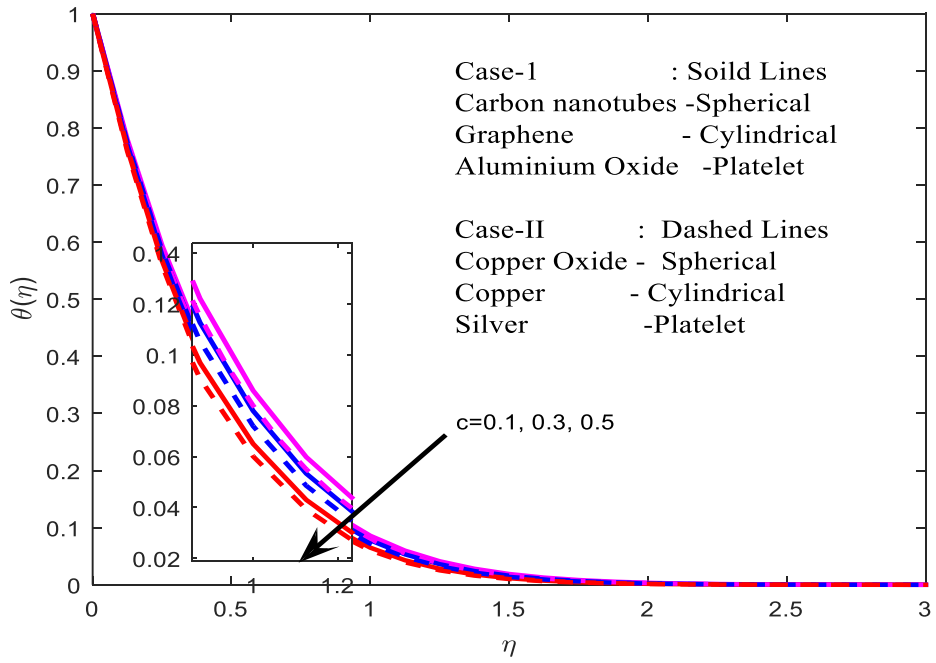

Figure 9. Temperature profiles for a variety of c values.

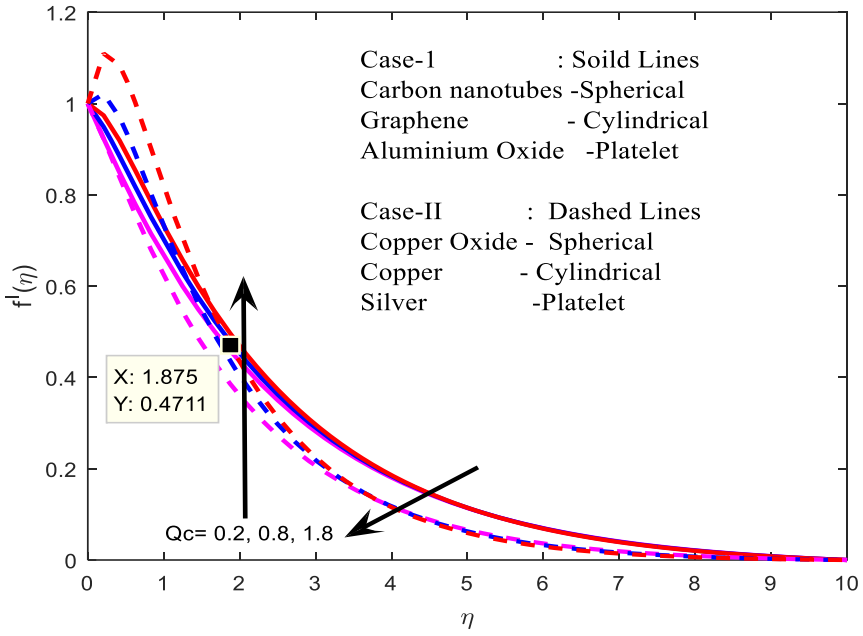

Figure 10. Velocity profiles for various Qc values.

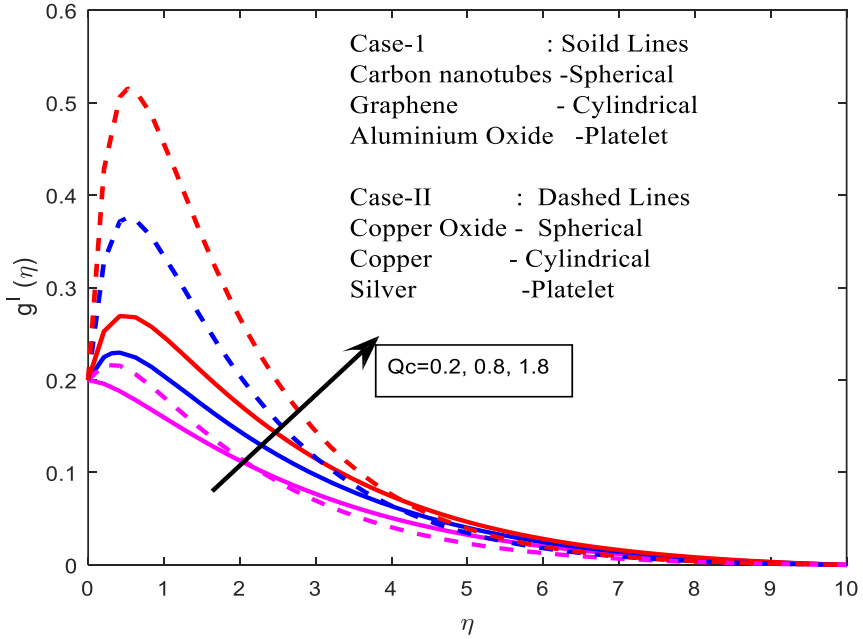

Figure 11. shows velocity profiles for various Qc values.

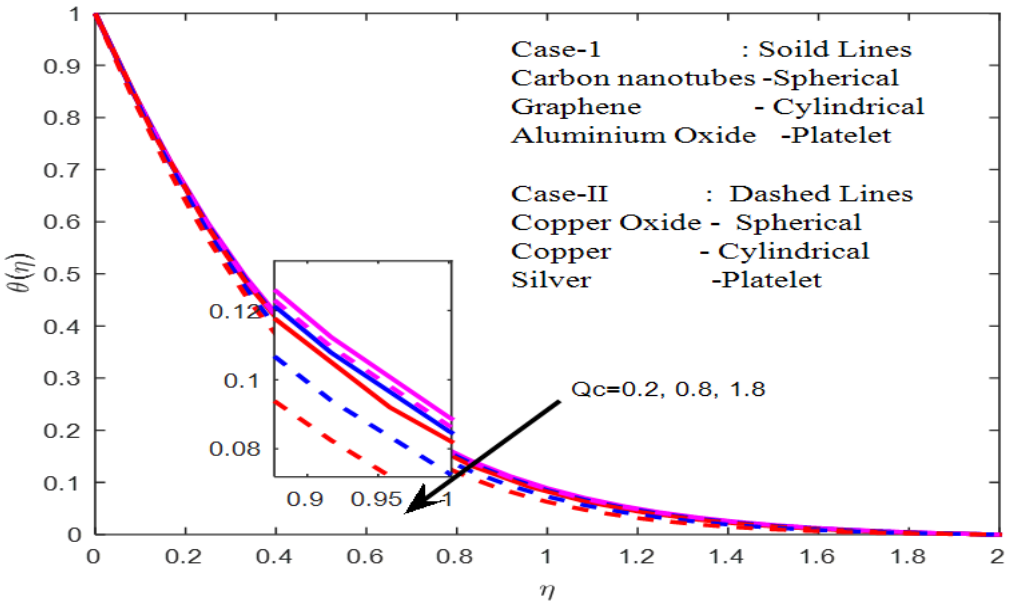

Figure 12. shows temperature profiles for various Qc values.

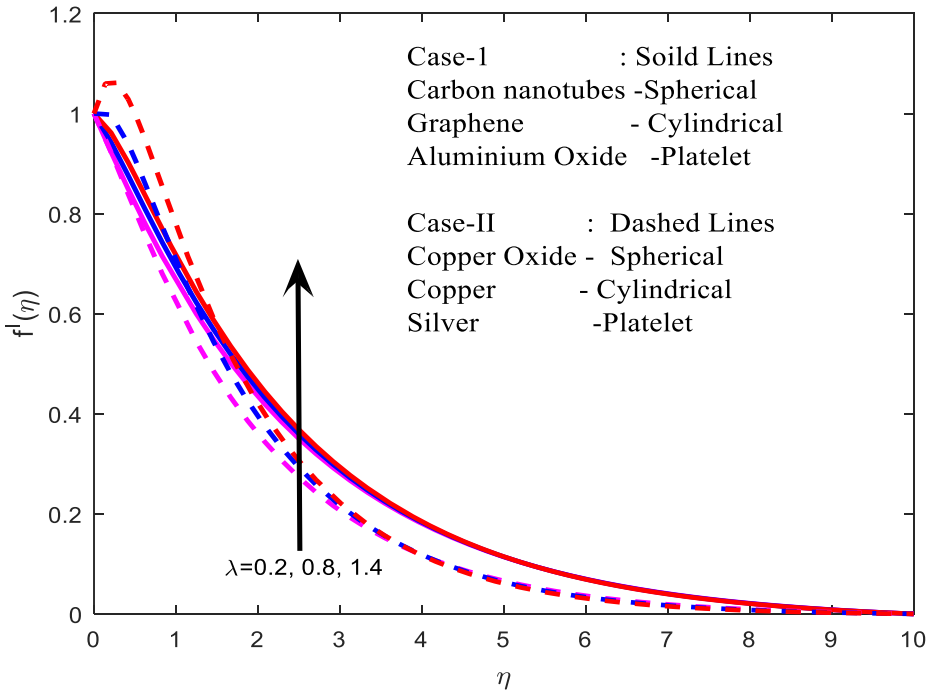

Figure 13. shows velocity profiles for various levels of λ.

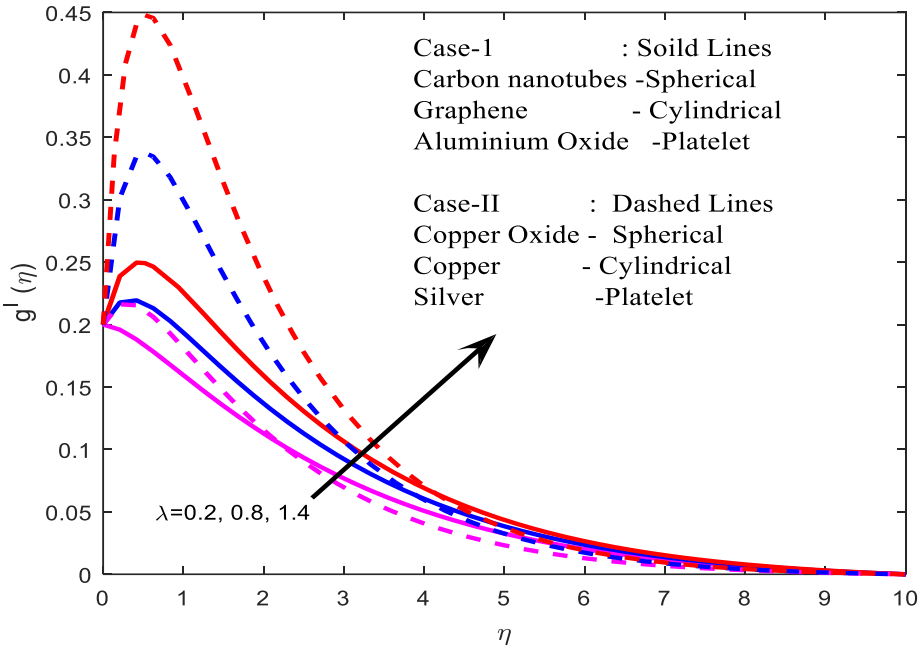

Figure 14. shows velocity profiles for various levels of λ.

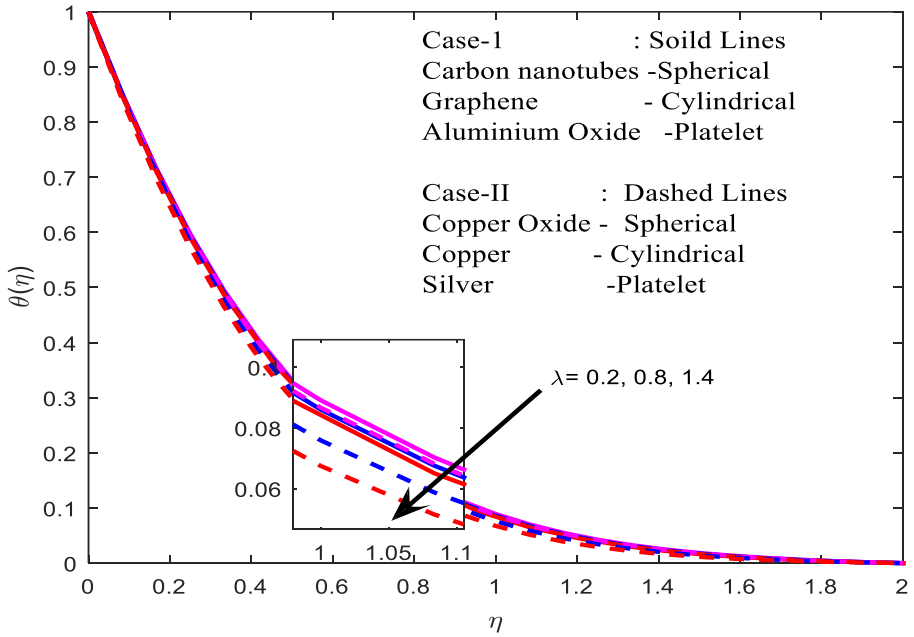

Figure 15. shows temperature curves for various levels of λ.

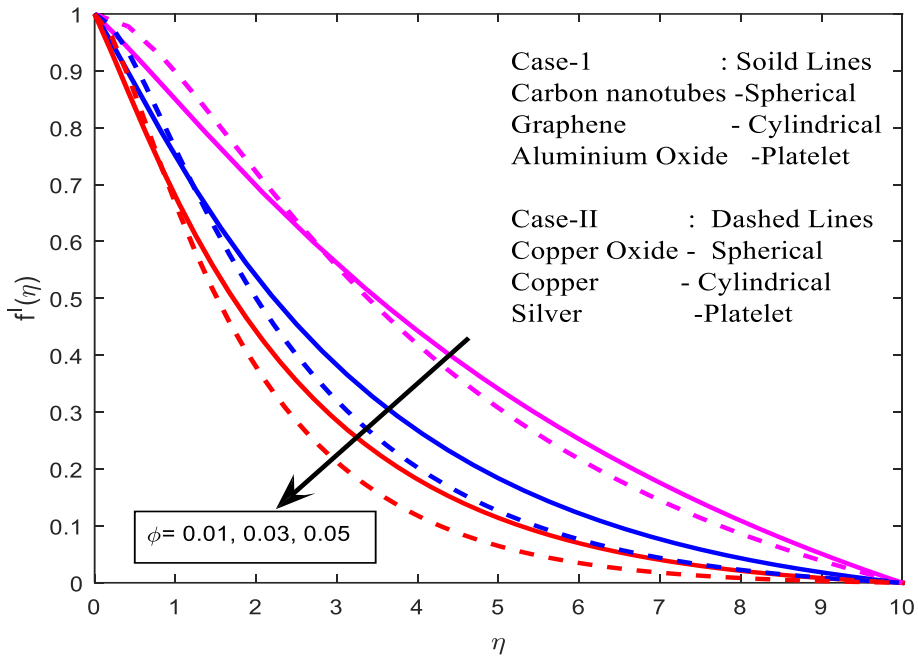

Figure 16. shows velocity profiles for various levels of φ.

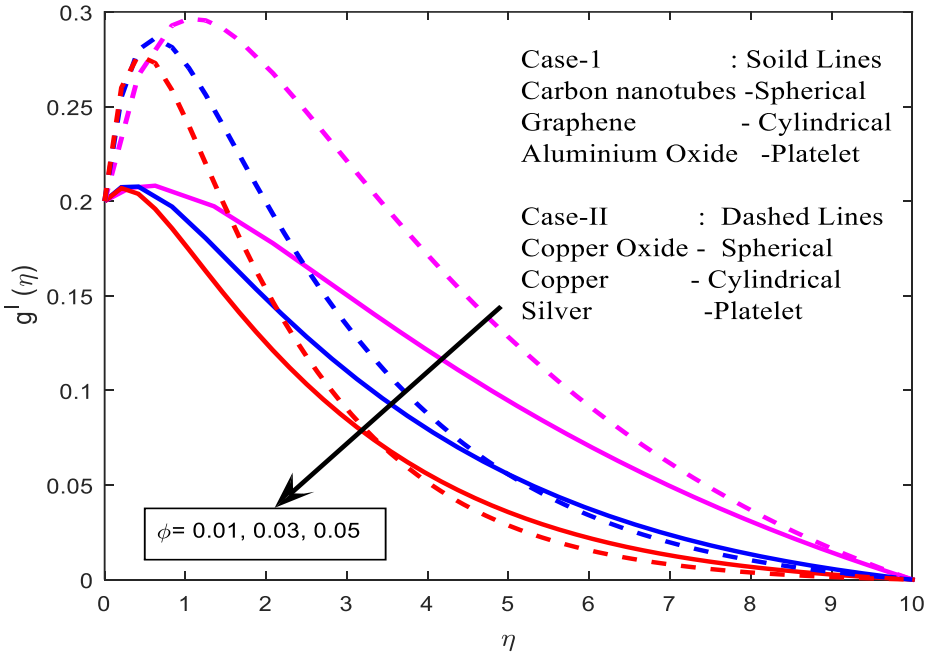

Figure 17. shows velocity profiles for various levels of φ.

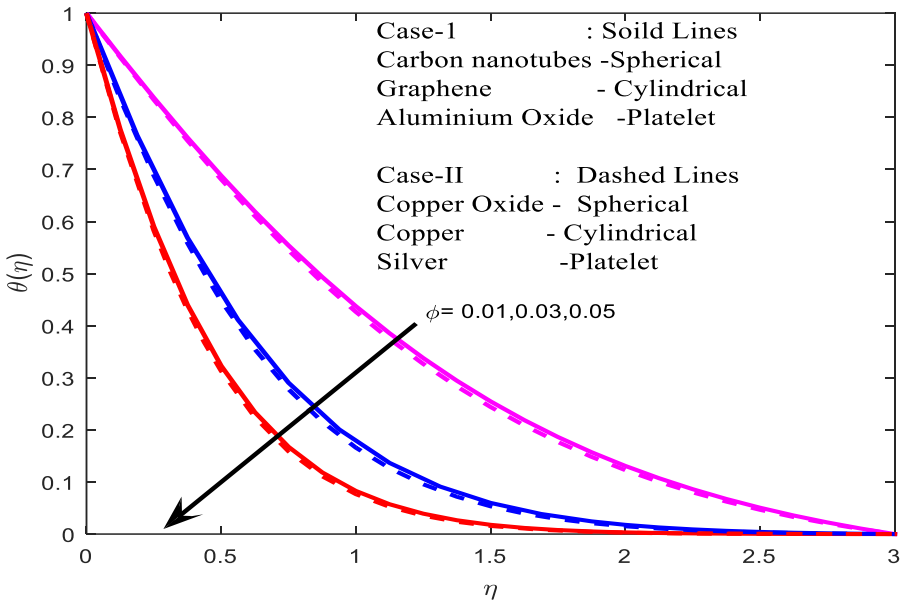

Figure 18. shows temperature curves for various levels of φ.

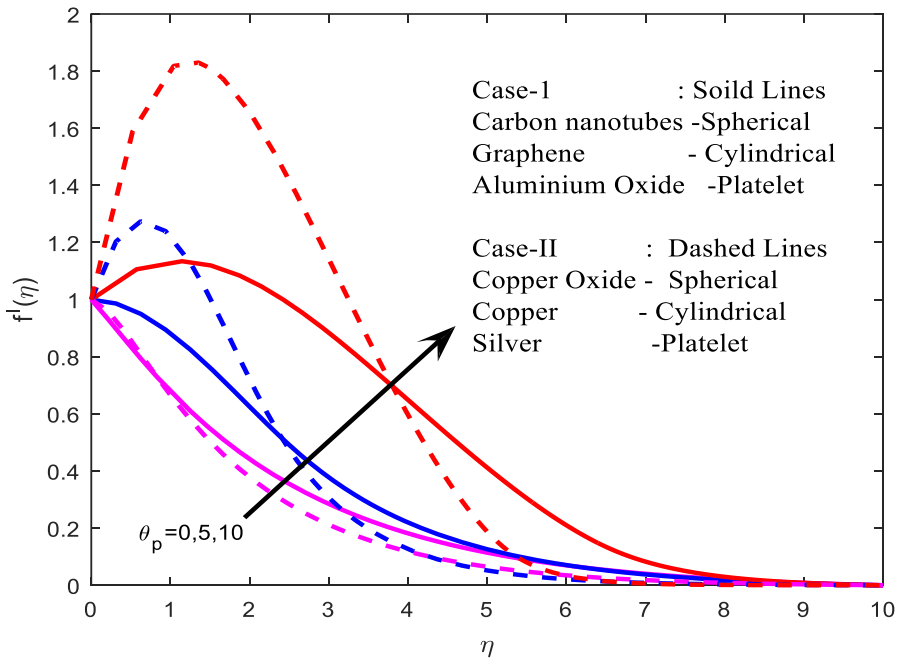

Figure 19. Velocity profiles for various θp values.

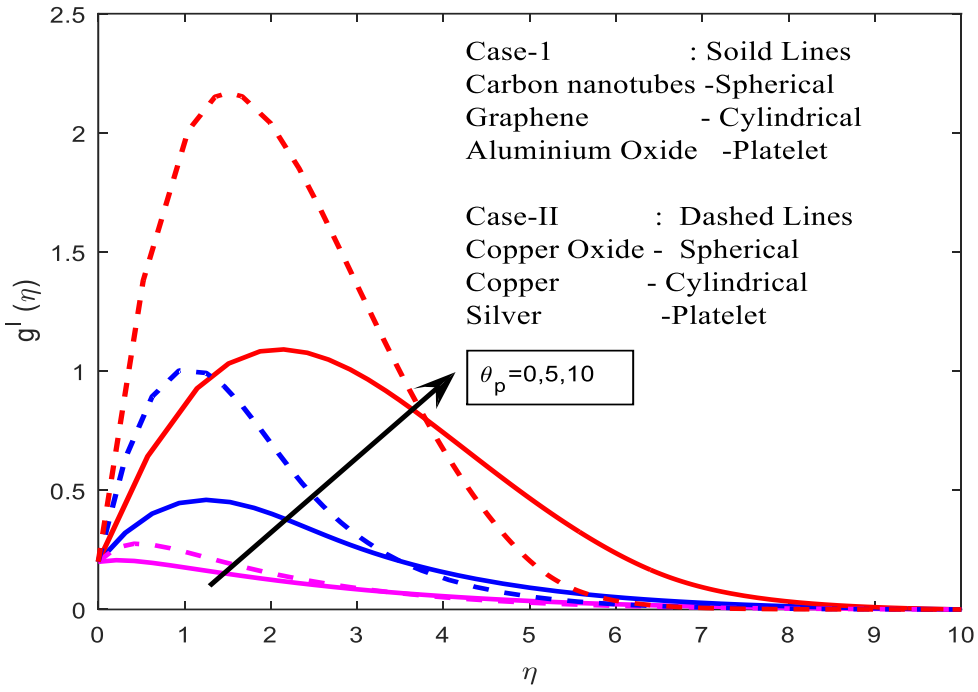

Figure 20. Velocity profiles for various θp values.

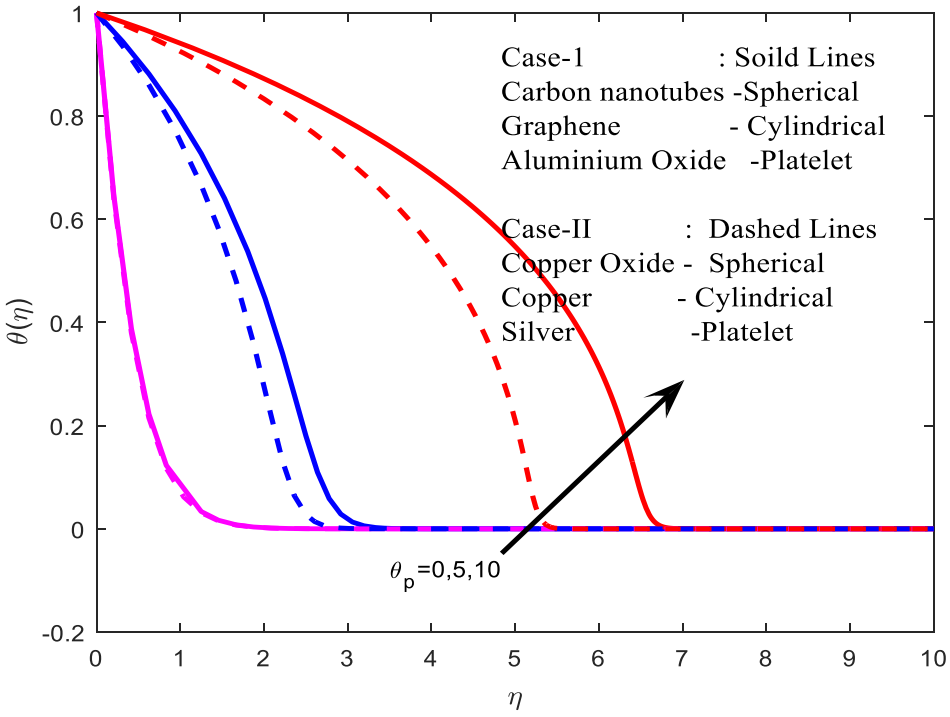

Figure 21. Temperature profiles for a variety of θp values.

4. Rate of friction and heat transfer

In Table 1 displays the Thermo physical quantities of nanoparticles with different shapes. Table 2 represents the variation in the skin friction coefficients at various non-dimensional governing parameters it is evident from the table that increasing the quadratic thermal radiation parameter R reduces the friction coefficient for case1 and increases the friction coefficient for case 2 in *x*- direction. But it increases the friction coefficient for both the cases in *y* directions. It is also interesting to mention that increasing the dimensionless suction velocity f_w reduces the friction coefficient for both the case x and *y* directions. A raise in Stretching rate ratio c reduces the friction coefficient for both the cases but oscillates the friction coefficient for case 1 and increases the friction coefficient for case 2 in *y* directions. It is also interesting to mention that increasing the nonlinear convection parameter Q_c, mixed convection parameter λ, and the temperature ratio parameter θ_p will increase the friction coefficient for both the cases in x and *y* directions. A raise in volume fraction of nanoparticles of the ternary cross breed nanofluid (ϕ) increases the friction coefficient for both the cases in *x* directions and increases the friction coefficient for the case 1 but it reduces the friction coefficient for case 2 in y directions.

Figure 22 (a–c) explains the surface plot of the skin friction with different parameters like radiation parameter, stretching rate ratio, and temperature ratio, with that Figure 22 (d–i) explains the surface plot of Nusselt number with the given parameters for both cases separately with different conditions like linear nonlinear and quadratic.

Table 3 represents the variation in the Nusselt number at various non-dimensional governing parameters. It is evident from the table that increasing the nonlinear convection parameter Q_c, the dimensionless suction velocity f_w, the quadratic thermal radiation parameter R, Stretching rate ratio c, and mixed convection parameter λ increases the Nusselt number for both solid particle 1 and solid particle 2 with linear, nonlinear and quadratic cases. It is also interesting to mention that a rise in the volume fraction of nanoparticles of the ternary cross breed nanofluid (ϕ) reduces the Nusselt number for both solid particle 1 and solid particle 2 with linear, nonlinear, and quadratic cases. It is also interesting to mention that increasing the temperature ratio parameter θ_p decreases the Nusselt number for both solid particle 1 and solid particle 2 with linear and quadratic cases. However, increases the Nusselt number for both solid particle 1 and solid particle 2 with the nonlinear case.

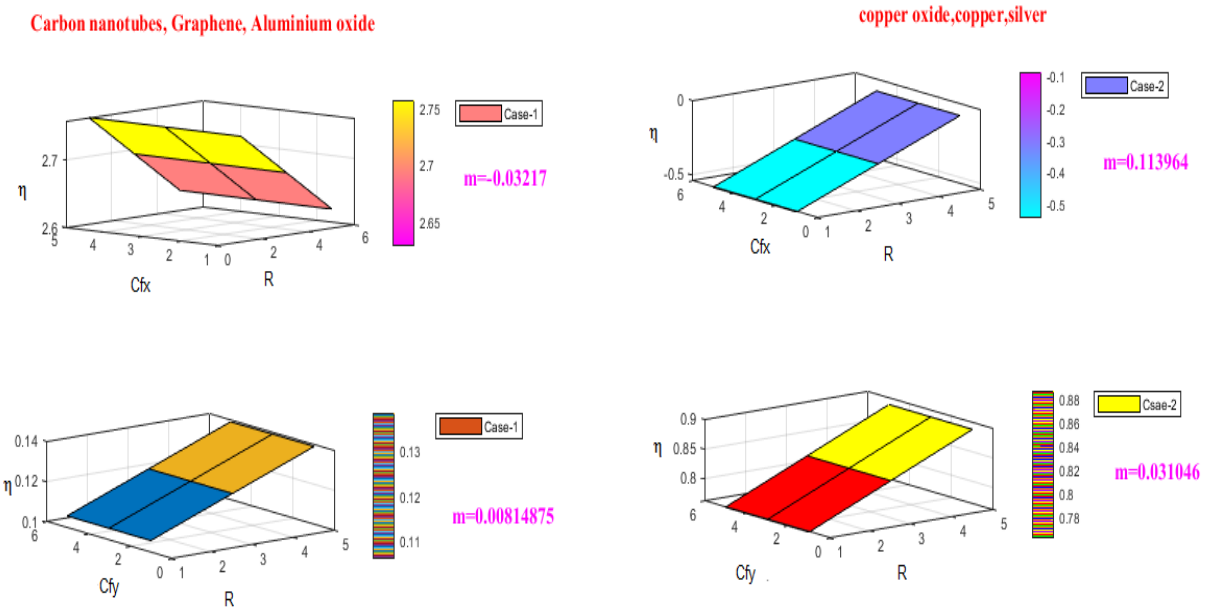

Figure 22(a). Surface plot of skin friction in x and y direction for radiation parameter with both the cases.

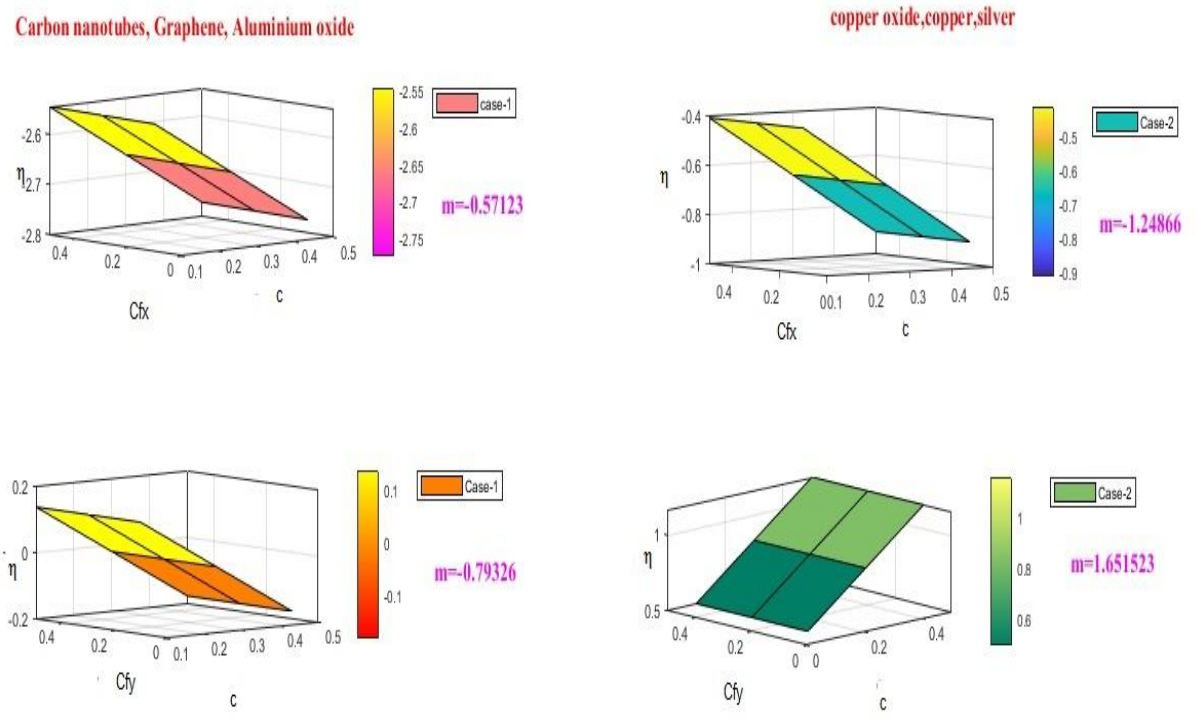

Figure 22(b). Surface plot of skin friction in x and y direction for Stretching rate ratio with both the cases.

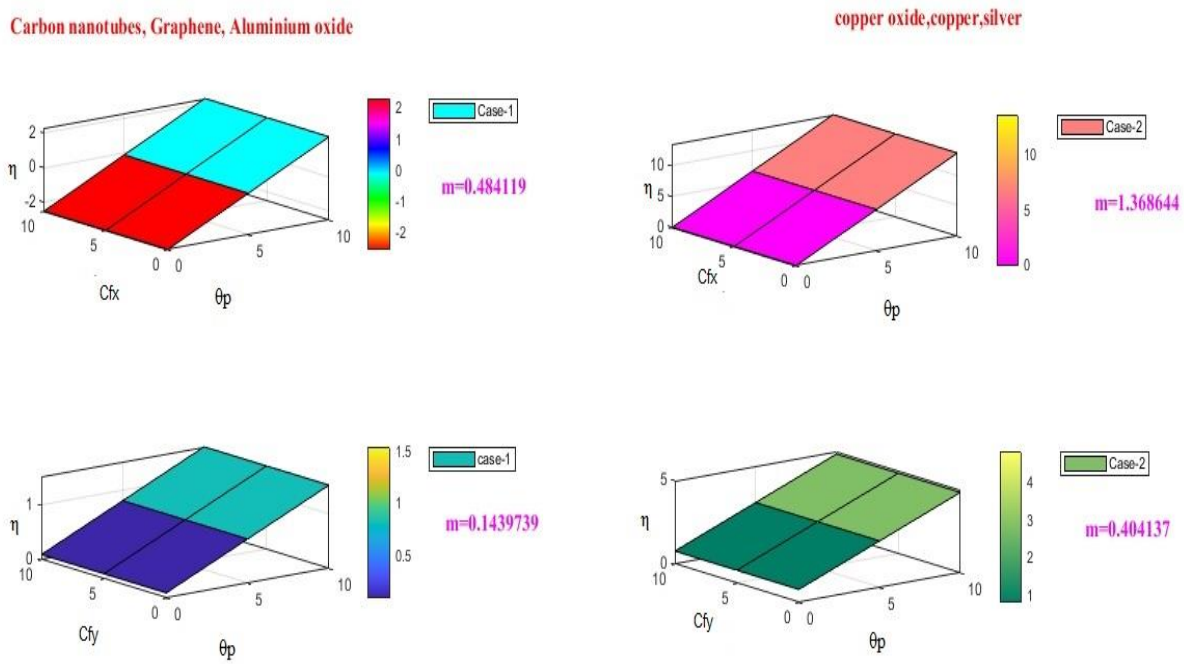

Figure 22(c). Surface plot of skin friction in x and y direction for temperature ratio with both the cases.

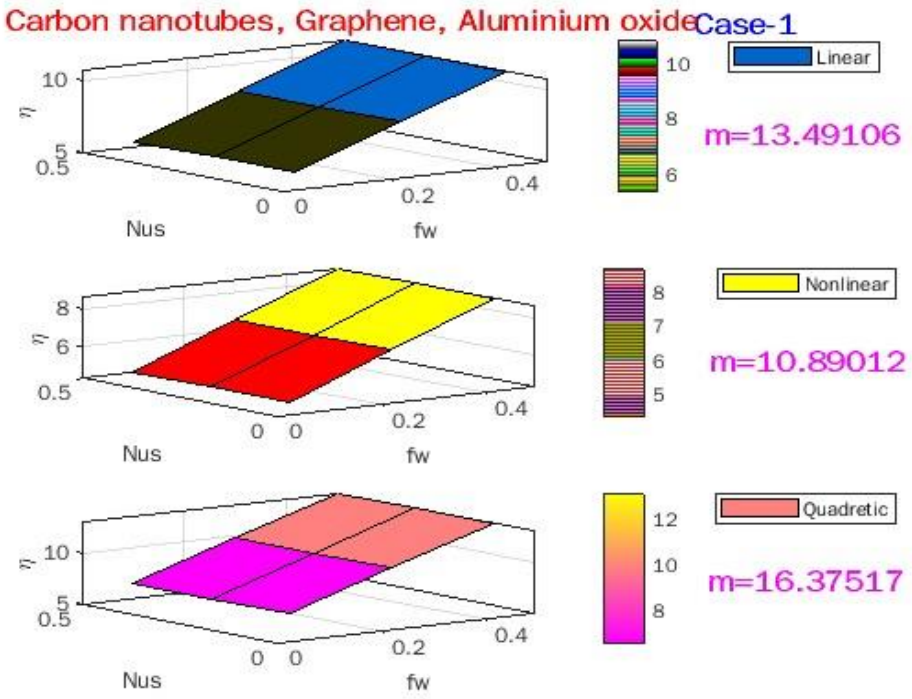

Figure 22(d). Surface plot of Nusselt number for dimensionless suction velocity in case1 with different conditions like linear nonlinear and quadratic.

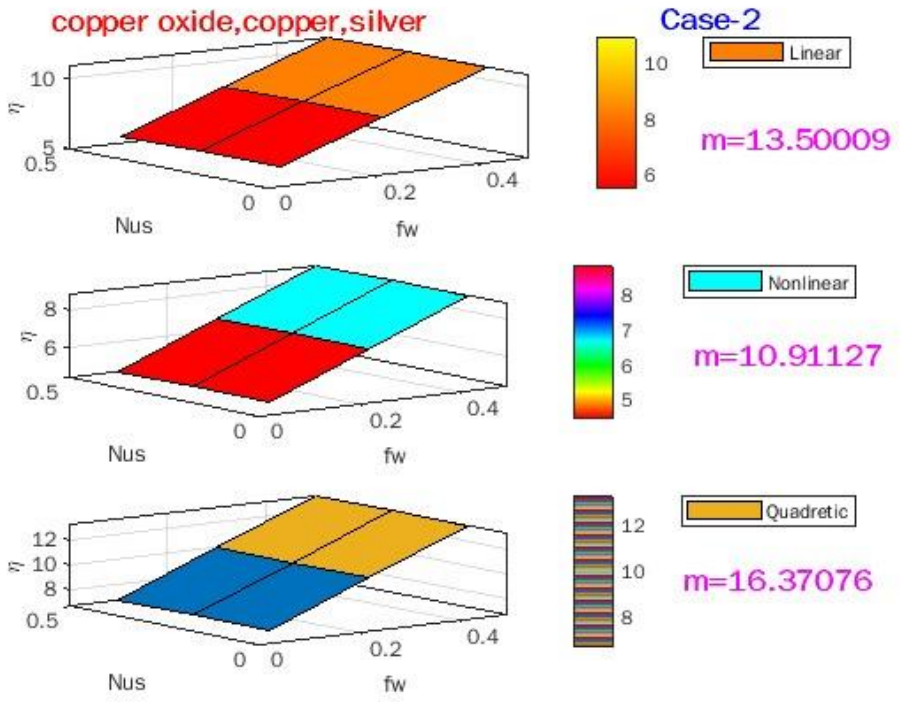

Figure 22(e). Surface plot **of** Nusselt number for dimensionless suction velocity in case2 with different conditions like linear nonlinear and quadratic.

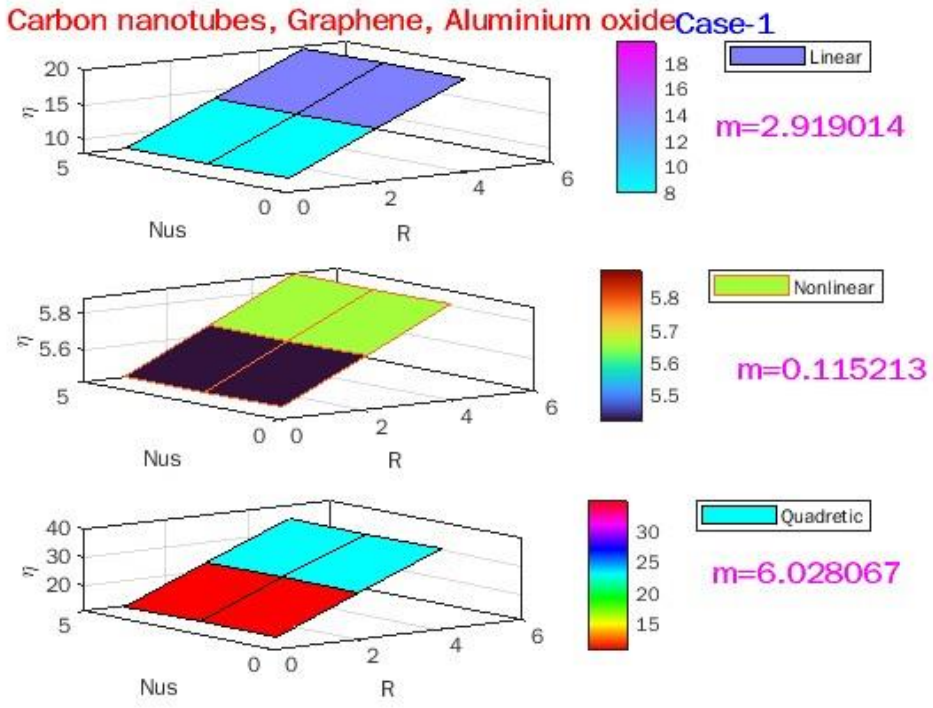

Figure 22(f). Surface plot of **Nusselt** number for radiation parameter in case1 with different conditions like linear nonlinear and quadratic.

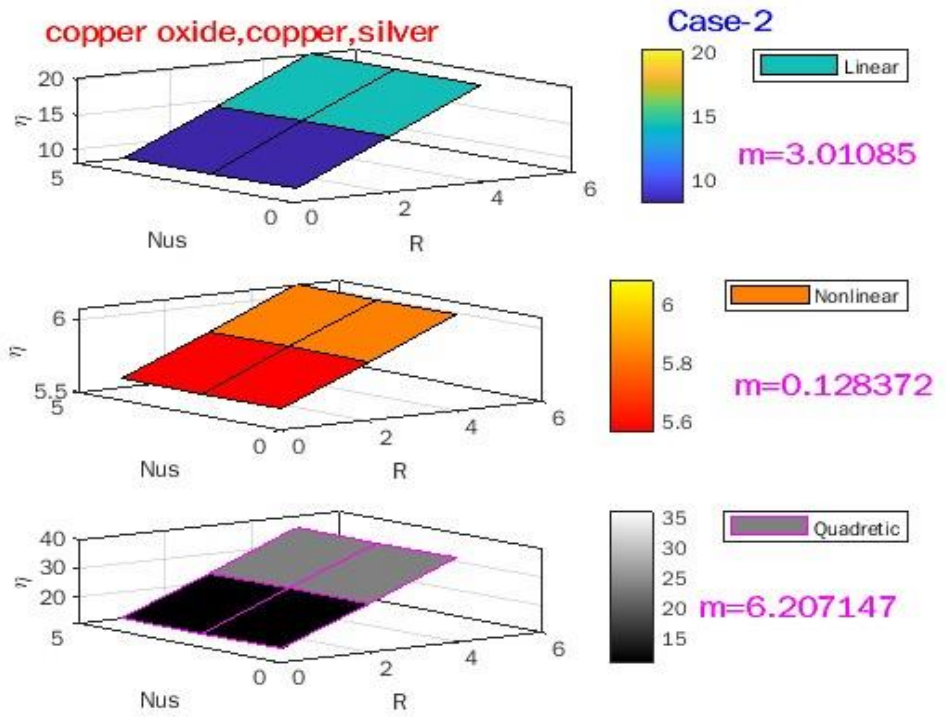

Figure 22(g). Surface plot of Nusselt number for radiation parameter in case2 with different conditions like linear nonlinear and quadratic.

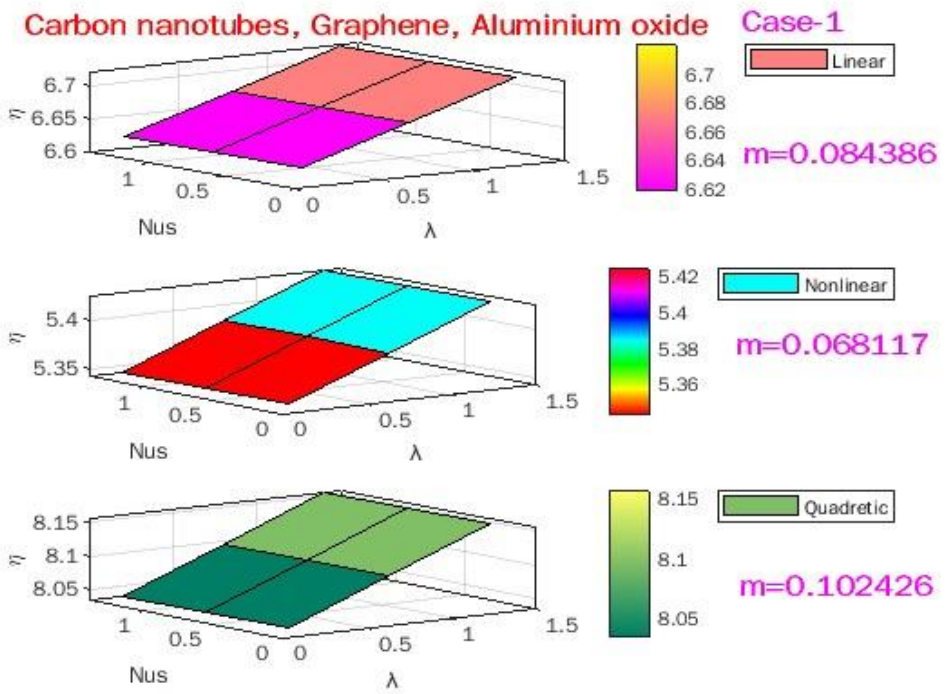

Figure 22(h). Surface plot of Nusselt number for mixed convection parameter in case1 with different conditions like linear nonlinear and quadratic.

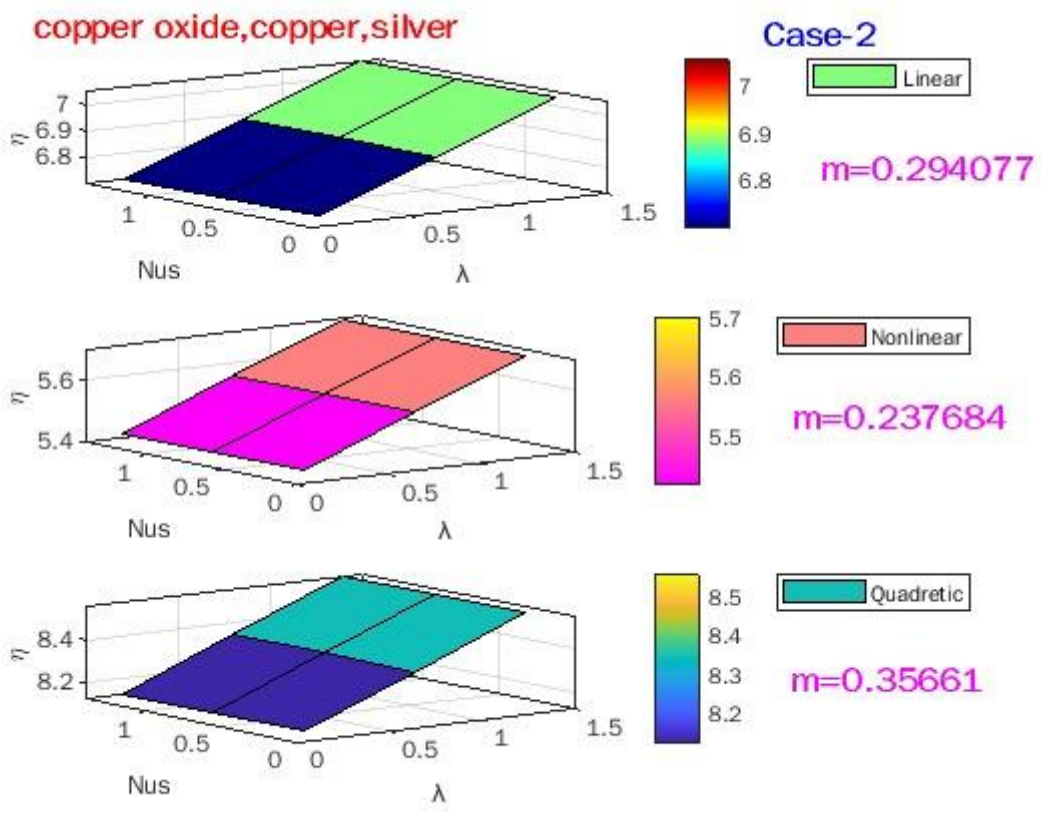

Figure 22(i). Surface plot of Nusselt number for mixed convection parameter in case2 with different conditions like linear nonlinear and quadratic.

Table 1. Sources of nanoparticles include density, thermal conductivity, and specific heat capacity of water, as well as the kinds and forms of nanoparticles.

	Nomenclature of nano-particles and base fluid	ρ (kg/m^3)	c_p (1/kgK)	k (W/mk)	Nanoparticle shapes
Base fluid	Water H_2O	997.1	4.179	0.623	
Ternary hybrid Nanofluid 1	Graphene	2200	790	5000	Cylindrical
	Carbon nanotubes	2100	410	3007.4	Spherical
	Aluminum oxide Al_2O_3	3970	765	40	Platelet
Ternary hybrid Nanofluid 2	Copper Cu	8933	385	400	Cylindrical
	Silver Ag	10,500	235	429	Platelet
	Copper(ll)oxide CuO	6500	535.6	20	Spherical

Table 2. The values of the skin friction coefficient and the local Nusselt number as physical parameters.

							Cfx		*Cfy*	
R	*fw*	*c*	*Qc*	λ	ϕ	θp	Case 1	Case2	Case 1	Case 2
1							2.758817	−0.546717	0.105776	0.761897
3							2.690748	−0.302658	0.122916	0.827886
5							−2.630133	−0.090861	0.138371	0.88608
	0.1						−2.327214	0.166235	0.154472	0.880765
	0.3						−2.831901	−1.127956	0.086732	0.65196
	0.5						−3.285035	−2.234385	0.03526	0.478692
		0.1					−2.555468	−0.427144	0.085641	0.420095
		0.3					−2.637750	−0.620172	0.086165	0.995654
		0.5					−2.783960	−0.926606	−0.231663	1.080704
			0.2				−3.176114	−2.87371	−0.00938	0.239065
			0.8				−1.620459	3.264017	0.32738	1.581922
			1.8				−0.104449	8.965899	0.654712	2.819509
				0.2			−3.176114	−2.87371	−0.00938	0.239065
				0.8			−2.005413	1.778223	0.244135	1.258072
				1.4			−0.857868	6.158694	0.492132	2.211135
					.01		−13.700995	−7.677303	−0.154679	1.252037
					.03		−4.998121	−1.709421	0.054646	0.90467
					.05		−3.379385	−1.070517	0.06261	0.699632
						0	−2.594291	−0.532185	0.116538	0.752381
						5	−0.025598	7.638196	0.780003	2.879964
						10	2.246901	13.154259	1.556277	4.79375

Table 3. Validation and reliability**:** comparative analysis of with Reddy Gorla et al. [34] and Wang [35].

Pr	Reddy Gorla et al. [34]	Wang [35]	Present results
0.2	0.1691	0.1691	0.169090104
2	0.9114	0.9114	0.911360012
7	1.8905	1.8954	1.895400102

5. Conclusions

In recent years, fluid mixtures have become more and more important in various systems, including medicinal treatments, industry, experimental instrument design, aerosol particle processing, and naval academies. The Rosseland approximation on 3D flow characteristics is nonlinear, linear, and quadratic due to the presence of Fourier flux and Boussinesq second order thermal variation. Ternary hybrid nanoparticle densities and various shapes are included. The governing system that results is then tweaked, and a solution with two different mixture compositions is shown (Case-I and Case-II). Graphene (Cylindrical), Carbon nanotubes (Spherical), and aluminum oxide (Platelet) were considered in the first mixture, whereas copper (Cylindrical), copper oxide (Spherical), and silver oxide (Platelet) were studied in the second mixture. Many changes in two mixture compositions, as well as linear,

quadratic, and nonlinear thermal radiation situations of the flow, have been discovered. The study's findings are presented in the following lines.

1. In comparison to Case-2 ternary combinations, the temperature distribution in Case-1 ternary mixtures is greater. When compared to a mixture of copper (Cylindrical), copper oxide (Spherical), and silver (Platelet), & a mixture of graphene (Cylindrical), carbon nanotubes (Spherical), and aluminum oxide (Platelet) has better conductivity.

2. In both cases, the volume percentage of nanoparticles lowered the temperature distributions.

3. In both cases of mixtures, the temperature ratio improves the temperature and velocities.

4. For both compositions, the quadratic convection parameter reduces the temperature and velocity distribution f' while increasing the radial velocity field g'.

5. For both compositions, the heat transfer rate is higher in quadratic thermal radiation than in linear and nonlinear radiation.

6. Because Case-II composition has a larger density than Case-I composition, the Local Nusselt number is higher in Case-II composition. This helps to increase particle interaction.

7. As quadratic convection increases, the heat transfer rate increases.

8. In copper oxide (Spherical), copper (Cylindrical), and silver (Platelet) compositions, the friction factor coefficient is much higher.

Further extensions

1. This can be extended by converting the model into bio-convection.
2. It also can extend by adding the different kinds of diffusivity properties and linear as well as nonlinear porous layers (Triple diffusion).
3. Second order, third order slips with variable properties can be included and studied using difference approximations.

Nomenclature

a	Rate of stretching for motion in the x-axis
Cf_y	(friction in y-direction) Coefficients of localized skin friction
$dg/d\eta$	The motion in the y-direction has a dimensionless horizontal velocity
$g(\eta)$	The motion in the y-direction has a dimensionless vertical velocity
Cf_x	(friction in x-direction) Coefficients of localized skin friction
$df/d\eta$	The motion in the x-direction has a dimensionless horizontal velocity
$f(\eta)$	The motion in the x-direction has a dimensionless vertical velocity
Nu	Nusselt number
λ	mixed convection parameter
η	Dimensionless distance
b	Stretching velocity for motion in the y-axis
f_w	Dimensionless suction velocity
κhnf	Thermal conductivity of the ternary hybrid nanofluid (W/m K)
$\theta(\eta)$	Dimensionless temperature
κbf	Thermal conductivity of the base fluid
$\theta_P = \frac{T_w}{T_\infty}$	is the temperature ratio parameter.

Re	Reynold number
c	Stretching rate ratio
$R=\frac{4\sigma^* T_\infty^3}{kk^*}$	is the quadratic thermal radiation parameter
Qc	is quadratic /nonlinear convection parameter
ρ_{bf}	The basefluid's density (kg/m^3)
$(\rho c_p)_{hnf}$	The ternary hybrid nanofluid's heat capacity (J/kgK)
ρ_{hnf}	The ternary hybrid nanofluid's density (kg/m^3)
T	The ternary hybrid nanofluid's dimensional temperature (K)
T_w	Temperature of the wall dimensions (K)
$T\infty$	Fluid temperature at a distance from the wall (K)
μ_3 and κ_3	Viscosity and thermal conductivity of a nanofluid with a platelet basis (*Ns/m^2 & W/m K*)
μ_2 and κ_2	Viscosity and thermal conductivity of a nanofluid with a cylindrical basis (*Ns/m^2 & W/m K*)
μ_1 and κ_1	Viscosity and thermal conductivity of a nanofluid with a spherical basis (*Ns/m^2 & W/m K*)
u	The motion's dimensional velocity in the x-direction (*m/s*)
u_w	The motion along the x-axis is being stretched at a faster rate. (*m/s*)
v	The motion's dimensional velocity in the y-direction ((*m/s*)
v_w	The motion along the y-axis is being stretched at a faster rate. *(m/s*)
μ_{hnf}	The ternary hybrid nanofluid's dynamic viscosity (*Ns/m^2*)
ϕ_3	platelet nanoparticles volume (*m^3)*
ϕ_2	cylindrical nanoparticles volume (*m^3*)
ϕ_1	spherical nanoparticles volume (*m^3*)
ϕ	The ternary hybrid nanofluid's volume percent (*m^3*)
$Q_c=\frac{\beta_1}{\beta_0}(T_w-T_\infty)$	Quadratic/nonlinear convection parameter
$\lambda=\frac{Gr_x}{\mathrm{Re}_x^2}=\frac{gb\beta_0}{a^2}$	The mixed convection parameter,

Acknowledgments

This research received funding support from the NSRF via the Program Management Unit for Human Resources & Institutional Development, Research and Innovation.

Conflict of interest

The authors declare no conflict of interest.

References

1. S. E. Ahmed, Z. A. S. Raizah, A. Chamkha, Mixed convective transport in inclined porous open arc-shaped enclosures saturated by nanofluids using a second-order Boussinesq approximation, *Case Stud. Therm. Eng.*, **27** (2021), 101295. https://doi.org/10.1016/j.csite.2021.101295

2. A. Ayub, Z. Sabir, D. Le, A. Aly. Ayman, Nanoscale heat and mass transport of magnetized 3-D chemically radiative hybrid nanofluid with orthogonal/inclined magnetic field along rotating sheet, *Case Stud. Therm. Eng.*, **26** (2021), 101193. https://doi.org/10.1016/j.csite.2021.101193
3. H. T. Basha, R. Sivaraj, V. R. Prasad, O. A. Beg, Entropy generation of tangent hyperbolic nanofluid flow over a circular cylinder in the presence of nonlinear Boussinesq approximation: A non-similar solution, *J. Therm. Anal. Calorim.,* **143** (2021), 2273–2289. https://doi.org/10.1007/s10973-020-09981-5
4. L. A. Dombrovsky, S. S. Sazhin, E. M. Sazhina, G. Feng, M. R. Heikal, M. E. A. Bardsley, et al., Heating and evaporation of semi-transparent diesel fuel droplets in the presence of thermal radiation, *Fuel*, **80** (2001), 1535–1544. https://doi.org/10.1016/S0016-2361(01)00025-4
5. H. M. Elshehabey, Z. Raizah, H. F. Öztop, S. E. Ahmed, MHD natural convective flow of Fe_3O_4-H_2O ferrofluids in an inclined partial open complex-wavy-walls ringed enclosures using non-linear Boussinesq approximation, *Int. J. Mech. Sci.*, **170** (2020), 105352. https://doi.org/10.1016/j.ijmecsci.2019.105352
6. M. D. Kumar, C. S. K. Raju, K. Sajjan, E. R. El-Zahar, N. A. Shah, Linear and quadratic convection on 3D flow with transpiration and hybrid nanoparticles, *Int. Comm. Heat Mass*, **134** (2022), 105995. https://doi.org/10.1016/j.icheatmasstransfer.2022.105995
7. V. P. Kabashnikov, G. I. Kmit. Effect of turbulent pulsations on thermal radiation from a medium in the quadratic approximation, *Inzhenerno Fizicheskii Zhurnal,* **37** (1979), 405–411. https://doi.org/10.1007/BF00861672
8. B. Mahanthesh, J. Mackolil, Flow of nanoliquid past a vertical plate with novel quadratic thermal radiation and quadratic Boussinesq approximation: Sensitivity analysis, Int. Comm. Heat Mass, **120** (2021), 105040. https://doi.org/10.1016/j.icheatmasstransfer.2020.105040
9. B. Mahanthesh, J. Mackolil, M. Radhika, W. Al-Kouz, Significance of quadratic thermal radiation and quadratic convection on boundary layer two-phase flow of a dusty nanoliquid past a vertical plate, *Int. Comm. Heat Mass.*, **120** (2021), 105029. https://doi.org/10.1016/j.icheatmasstransfer.2020.105029
10. N. A. Shah, A. Wakif, E. R. El-Zahar, S. Ahmad, S. J. Yook, Numerical simulation of a thermally enhanced EMHD flow of a heterogeneous micropolar mixture comprising (60%)-ethylene glycol (EG), (40%)-water (W), and copper oxide nanomaterials (CuO), *Case Stud. Therm. Eng.,* **35** (2022), 102046. https://doi.org/10.1016/j.csite.2022.102046
11. T. Elnaqeeb, I. L. Animasaun, N. A. Shah, Ternary-hybrid nanofluids: significance of suction and dual-stretching on three-dimensional flow of water conveying nanoparticles with various shapes and densities, *Zeitschrift für Naturforschung A*, **76** (2021), 231–243. https://doi.org/10.1515/zna-2020-0317
12. W. Al-Kouz, B. Mahanthesh, M. S. Alqarni, K. Thriveni, A study of quadratic thermal radiation and quadratic convection on viscoelastic material flow with two different heat source modulations, *Int. Comm. Heat Mass.,* **126** (2021), 105364. https://doi.org/10.1016/j.icheatmasstransfer.2021.105364
13. B. Mahanthesh, Quadratic radiation and quadratic Boussinesq approximation on hybrid nanoliquid flow, In: *Mathematical Fluid Mechanics*, (2021), 13–54. https://doi.org/10.1515/9783110696080-002
14. T. Muhammad, H. Waqas, U. Farooq, M. S. Alqarni, Numerical simulation for melting heat transport in nanofluids due to quadratic stretching plate with nonlinear thermal radiation, *Case Stud. Therm. Eng.*, **27** (2021), 101300. https://doi.org/10.1016/j.csite.2021.101300

15. P. Naveen, C. RamReddy, Soret and viscous dissipation effects on MHD flow along an inclined channel: Nonlinear Boussinesq approximation, In: *Numerical Heat Transfer and Fluid Flow*, 267–274. Springer, Singapore, 2019. https://doi.org/10.1007/978-981-13-1903-7_31
16. E. C. Okonkwo, I. Wole-Osho, I. W. Almanassra, Y. M. Abdullatif, T. Al-Ansari, An updated review of nanofluids in various heat transfer devices, *J. Therm. Anal. Calorim.*, **145** (2021), 2817–2872. https://doi.org/10.1007/s10973-020-09760-2
17. G. Palani, I. A. Abbas, Free convection MHD flow with thermal radiation from an impulsively-started vertical plate, *Nonlinear Anal-Model.,* **14** (2009), 73–84. https://doi.org/10.15388/NA.2009.14.1.14531
18. D. Srinivasacharya, C. RamReddy, P. Naveen, Effects of nonlinear Boussinesq approximation and double dispersion on a micropolar fluid flow under convective thermal condition, *Heat Transf.-Asian Re.*, **48** (2019), 414–434. https://doi.org/10.1002/htj.21391
19. K. Thriveni, B. Mahanthesh, Optimization and sensitivity analysis of heat transport of hybrid nanoliquid in an annulus with quadratic Boussinesq approximation and quadratic thermal radiation, *Eur. Phys. J. Plus*, **135** (2020), 1–22. https://doi.org/10.1140/epjp/s13360-020-00484-8
20. K. Thriveni, B. Mahanthesh, Nonlinear Boussinesq buoyancy driven flow and radiative heat transport of magnetohybrid nanoliquid in an annulus: A statistical framework, *Heat Transfer*, **49** (2020), 4759–4782. https://doi.org/10.1002/htj.21851
21. Z. A. Zainal, R. Nazar, K. Naganthran, I. Pop, Stability analysis of MHD hybrid nanofluid flow over a stretching/shrinking sheet with quadratic velocity, *Alex. Eng. J.,* **60** (2021), 915–926. https://doi.org/10.1016/j.aej.2020.10.020
22. M. Dostalík, C. Matyska, V. Průša, Weakly nonlinear analysis of Rayleigh–Bénard convection problem in extended Boussinesq approximation, *Appl. Math. Comput.,* **408** (2021), 126374. https://doi.org/10.1016/j.amc.2021.126374
23. B. K. Jha, M. O. Oni, Theory of fully developed mixed convection including flow reversal: A nonlinear Boussinesq approximation approach, *Heat Transf.-Asian Re.*, **48** (2019), 3477–3488. https://doi.org/10.1002/htj.21550
24. P. K. Kameswaran, B. Vasu, P. V. S. N. Murthy, R. S. R. Gorla, Mixed convection from a wavy surface embedded in a thermally stratified nanofluid saturated porous medium with non-linear Boussinesq approximation, *Int. Comm. Heat Mass*, **77** (2016), 78–86. https://doi.org/10.1016/j.icheatmasstransfer.2016.07.006
25. M. Krishnani, D. N. Basu, On the validity of Boussinesq approximation in transient simulation of single-phase natural circulation loops, *Int. J. Therm. Sci.,* **105** (2016), 224–232. https://doi.org/10.1016/j.ijthermalsci.2016.03.004
26. J. O. Olabode, A. S. Idowu, M. T. Akolade, E. O. Titiloye, Unsteady flow analysis of Maxwell fluid with temperature dependent variable properties and quadratic thermo-solutal convection influence, *Partial Differential Equations Appl. Math.,* **4** (2021), 100078. https://doi.org/10.1016/j.padiff.2021.100078
27. S. O. Opadiran, S. S. Okoya, Importance of convective boundary layer flows with inhomogeneous material properties under linear and quadratic Boussinesq approximations around a horizontal cylinder, *Heliyon*, **7** (2021), e07074. https://doi.org/10.1016/j.heliyon.2021.e07074
28. C. RamReddy, P. Naveen, D. Srinivasacharya, Influence of non-linear Boussinesq approximation on natural convective flow of a power-law fluid along an inclined plate under convective thermal boundary condition, *Nonlinear Eng.*, **8** (2019), 94–106. https://doi.org/10.1515/nleng-2017-0138

29. P. Rana, W. Al-Kouz, B. Mahanthesh, J. Mackolil. Heat transfer of TiO_2−EG nanoliquid with active and passive control of nanoparticles subject to nonlinear Boussinesq approximation, *Int. Comm. Heat Mass.*, **126** (2021), 105443. https://doi.org/10.1016/j.icheatmasstransfer.2021.105443
30. B. Vasu, R. S. R. Gorla, O. A. Bég, P. V. S. N. Murthy, V. R. Prasad, A. Kadir, Unsteady flow of a nanofluid over a sphere with nonlinear Boussinesq approximation, *J. Therm. Heat Transfer,* **33** (2019), 343–355. https://doi.org/10.2514/1.T5516
31. W. Prandtl, Über Flussigkeitsbewegung bei sehr kleiner Reibung, Verhandl. III, Internat. Math.-Kong., Heidelberg, Teubner, Leipzig, **1904** (1904), 484–491.
32. G. Ramesh, J. K. Madhukesh, R. Das, N. A. Shah, S. J. Yook, Thermodynamic activity of a ternary nanofluid flow passing through a permeable slipped surface with heat source and sink, *Waves Random Complex.*, 2022. https://doi.org/10.1080/17455030.2022.2053237
33. N. A. Shah, I. L. Animasaun, A. Wakif, O. K. Koriko, R. Sivaraj, K. S. Adegbie, et al., Significance of suction and dual stretching on the dynamics of various hybrid nanofluids: Comparative analysis between type I and type II models, *Phys. Scripta*, **95** (2020), 095205. https://doi.org/10.1088/1402-4896/aba8c6
34. R. Gorla, R. Subba, I. Sidawi, Free convection on a vertical stretching surface with suction and blowing, *Appl. Sci. Res.,* **52** (1994), 247–257. https://doi.org/10.1007/BF00853952
35. C. Y. Wang, Free convection on a vertical stretching surface, *ZAMM Z. Angew. Math. Mech.*, **69** (1989), 418–420. https://doi.org/10.1002/zamm.19890691115
36. P. Rana, G. Gupta, Heat transfer optimization of Marangoni convective flow of nanofluid over an infinite disk with Stefan blowing and slip effects using Taguchi method, *Int. Comm. Heat Mass,* **130** (2022), 105822. https://doi.org/10.1016/j.icheatmasstransfer.2021.105822
37. P. Rana, G. Gupta, Numerical and sensitivity computations of three-dimensional flow and heat transfer of nanoliquid over a wedge using modified Buongiorno model, *Comput. Math. Appl.,* **101** (2021), 51–62. https://doi.org/10.1016/j.camwa.2021.09.010
38. C. S. K. Raju, N. A. Ahammad, K. Sajjan, N. A. Shah, S. J. Yook, M. D. Kumar, Nonlinear movements of axisymmetric ternary hybrid nanofluids in a thermally radiated expanding or contracting permeable Darcy Walls with different shapes and densities: Simple linear regression, *Int. Comm. Heat Mass,* **135** (2022), 106110. https://doi.org/10.1016/j.icheatmasstransfer.2022.106110
39. P. Rana, W. Al-Kouz, B. Mahanthesh, J. Mackolil, Heat transfer of TiO_2-EG nanoliquid with active and passive control of nanoparticles subject to nonlinear Boussinesq approximation, *Int. Comm. Heat Mass,* **126** (2021), 105443. https://doi.org/10.1016/j.icheatmasstransfer.2021.105443
40. P. Rana, G. Gupta. FEM Solution to quadratic convective and radiative flow of Ag-MgO/H_2O hybrid nanofluid over a rotating cone with Hall current: Optimization using Response Surface Methodology, *Math. Comput. Simul.,* **201** (2022), 121–140. https://doi.org/10.1016/j.matcom.2022.05.012
41. M. K. B. Gratuito, T. Panyathanmaporn, R. A. Chumnanklang, N. B. Sirinuntawittaya, A. Dutta, Production of activated carbon from coconut shell: Optimization using response surface methodology, *Bioresource Technol.,* **99** (2008), 4887–4895. https://doi.org/10.1016/j.biortech.2007.09.042

42. P. Rana, S. Gupta, G. Gupta, Unsteady nonlinear thermal convection flow of MWCNT-MgO/EG hybrid nanofluid in the stagnation-point region of a rotating sphere with quadratic thermal radiation: RSM for optimization, *Int. Comm. Heat Mass*, **134** (2022), 106025. https://doi.org/10.1016/j.icheatmasstransfer.2022.106025
43. M. A. Bezerra, R. E. Santelli, E. P. Oliveira, L. S. Villar, L. A. Escaleira, Response surface methodology (RSM) as a tool for optimization in analytical chemistry, *Talanta,* **76** (2008), 965–977. https://doi.org/10.1016/j.talanta.2008.05.019

AIMS Press